Current Plant Biology 47 (2026) 100613

Contents lists available at ScienceDirect

Current Plant Biology

journal homepage: www.elsevier.com/locate/cpb

Diversity of photosynthesis-related and high-throughput phenotyping traits in indica rice

Hsiang-Chun Lin [a,b,*,1], Jacqueline Dionora [a], Dmytro Chebotarov [a,2], Ma Rebecca Laza [a], Ma. Elizabeth B. Naredo [a,c], Pauline A. Muyco [a], Stephen Klassen [a], Amelia Henry [a,g,3], W. Paul Quick [a,d,*], Kenneth L. McNally [a,e,f,*,4]

[a] International Rice Research Institute (IRRI), Los Baños, Philippines
[b] Department of Agronomy, National Taiwan University, Taipei, Taiwan
[c] Philippine Coconut Authority - Albay Research Center, Guinobatan, Albay 4503, Philippines
[d] Department of Animal and Plant Sciences, University of Sheffield, Sheffield S10 2TN, United Kingdom
[e] Philippine Genome Center for Agriculture, University of the Philippines Los Baños, College, Los Baños, Laguna 4031, Philippines
[f] Food Crops Research Institute, Yunnan Academy of Agricultural Sciences, Kunming 650200, China
[g] CIRAD, UMR AGAP Institut, Montpellier F-34398, France

ARTICLE INFO

Keywords:
Rice
High Throughput Phenotyping
GWAS
Stomatal density
Photosynthesis
Agronomic traits

ABSTRACT

Manual phenotyping of photosynthesis-related traits in rice is labor-intensive and limits the scale and temporal resolution of genetic analysis under field conditions. Here, we integrated unmanned aerial vehicle (UAV)-based high-throughput phenotyping (HTP) with genome-wide association studies (GWAS) to dissect the diversity and genetic architecture of photosynthesis-related traits in a large indica rice diversity panel (>300 accessions) evaluated across three dry seasons. A total of 45 traits, including UAV-derived NDVI, canopy height, and canopy temperature, together with leaf gas-exchange, stomatal, anatomical, and agronomic traits, were quantified. UAV-derived traits captured temporal growth and senescence dynamics and showed strong and consistent correlations with leaf photosynthetic rate, stomatal conductance, flowering time, biomass, and grain yield. GWAS identified multiple QTLs for photosynthetic and HTP traits, including a cross-year stable transpiration-rate QTL (qTRMMOL-2–2) and a photosynthetic-rate QTL (qPHOTO-1–2). Haplotype analyses revealed that the wall-associated receptor-like kinase gene *OsWAK6* and the potassium transporter gene *OsHAK1* were strongly associated with variation in photosynthetic rate and transpiration, respectively. Several elite accessions with consistently high photosynthetic performance carried superior haplotypes at multiple qPHOTO loci, suggesting their potential value for breeding. Together, our results demonstrate that UAV-based HTP provides reliable field-scale proxies for physiological performance, and that integrating HTP with GWAS can enable the identification of genetic targets for improving photosynthesis, water use, and yield potential in rice.

1. Introduction

By 2050, demand for cereal grain is likely to increase by 50% [1]; meeting this demand is currently unfeasible given that the annual increase in rice yields resulting from genetic improvement is currently less than 1% [2]. Meanwhile, ongoing climate change is affecting global temperature and rainfall patterns, resulting in significant challenges to food security. It is widely recognized that improvements in radiation use efficiency and photosynthetic performance are credible ways of closing the yield gap [3–6]. This is likely to be achieved through targeted

* Corresponding authors at: International Rice Research Institute (IRRI), Los Baños, Philippines.
E-mail addresses: hclin89@ntu.edu.tw (H.-C. Lin), m.dionora@usls.edu.ph (J. Dionora), d.chebotarov@cgiar.org (D. Chebotarov), mrclaza@gmail.com (M.R. Laza), mebnaredo@gmail.com (Ma.E.B. Naredo), p.muyco@cgiar.org (P.A. Muyco), stephen.p.klassen@gmail.com (S. Klassen), amelia.henry@cirad.fr (A. Henry), paulquick2323@gmail.com (W.P. Quick), kenmcn59@gmail.com (K.L. McNally).
[1] ORCID 0000-0003-1108-2622
[2] ORCID 0000-0003-1351-9453
[3] ORCID 0000-0001-6255-5480
[4] ORCID 0000-0002-9613-5537

https://doi.org/10.1016/j.cpb.2026.100613
Received 18 August 2025; Received in revised form 10 April 2026; Accepted 18 April 2026
Available online 20 April 2026
2214-6628/© 2026 The Authors. Published by Elsevier B.V. This is an open access article under the CC BY license (http://creativecommons.org/licenses/by/4.0/).

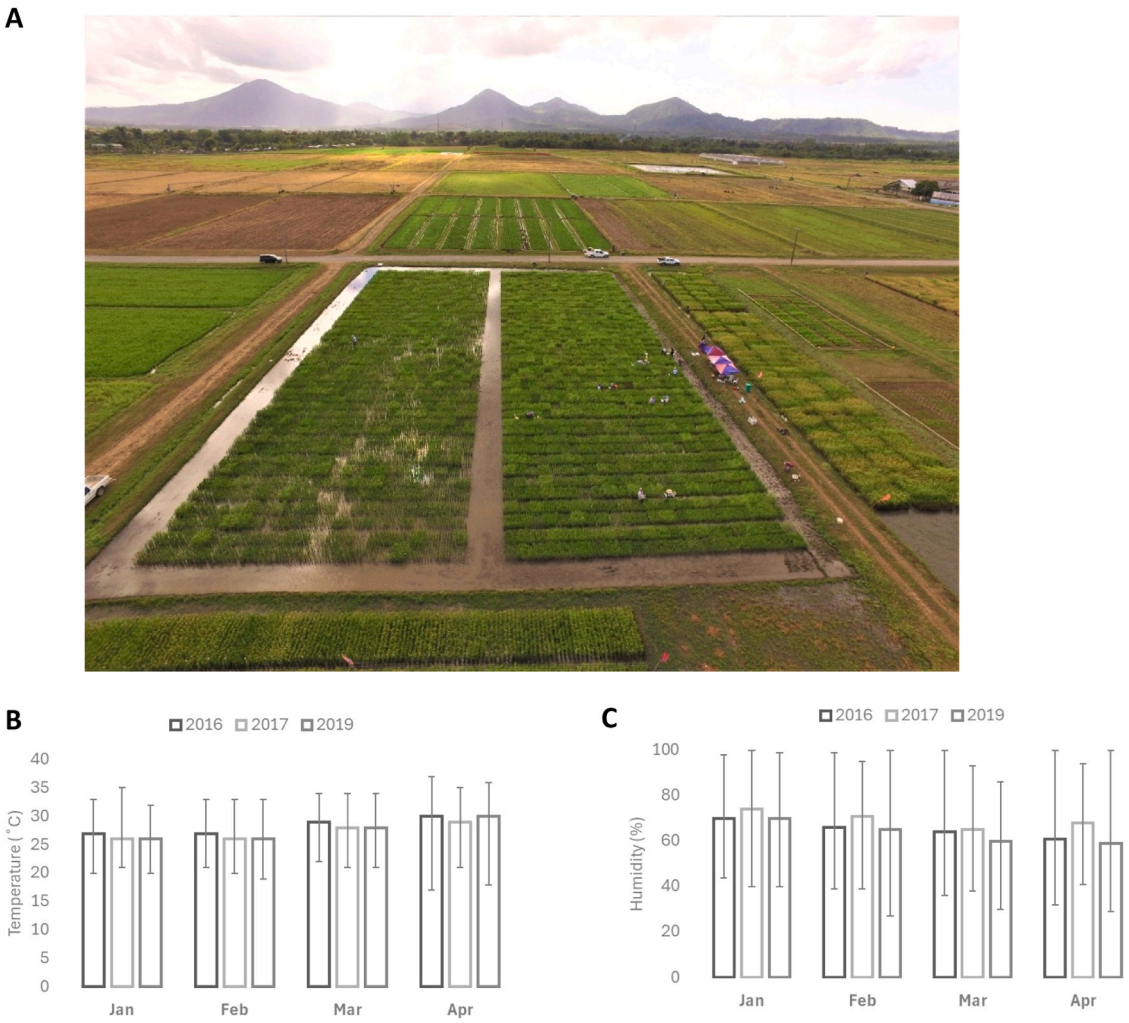

Fig. 1. (A) Images of the fields in 2016. (B) The average temperature during the growing months in 2016, 2017, and 2019. (C) The average humidity during the growing months in 2016, 2017, and 2019. The error bars indicate the highest and lowest values for each month.

genetic manipulation of key photosynthetic processes, driving the current interest in understanding the genetic determinants of photosynthetic capacity [7,8]. Several potential approaches to enhance photosynthetic efficiency, along with experiments involving elevated levels of CO_2, have demonstrated a yield benefit where increased photosynthesis is observed in food crops [9–11]. Natural genetic variation of photosynthetic capacity already exists within plant populations, providing the potential for enhancing photosynthetic abilities through genetic approaches. For example, Australian and Mexican wheat varieties displayed a significant link between rising CO_2 assimilation rates and genetic improvement in yield over successive release years, indicating that breeding efforts have inadvertently favored higher rates of photosynthesis [12,13]. Modern japonica rice varieties exhibited a higher net CO_2 assimilation rate than landraces, while linkages between photosynthetic rates and release years were not significant (Honda et al., 2024). The natural variation found in wild and cultivated rice varieties also offers a valuable and extensively resource for studying photosynthetic performance [14–16]. Harnessing this diversity will require effective strategies and tools to fully unlock its genetic potential.

The 3000 Rice Genome Project (3 K RG project) released the sequences of 3000 rice genomes [17]. This dataset enables the identification of genetic variation within known genes and its association with phenotypic diversity, thereby allowing the genetic dissection of traits with established phenotypic variation. What is now needed is trait information to help assign function to unknown genes and assess how variation at the genetic level is related to phenotypes under field conditions. Collecting this phenotypic data using traditional methodologies is labor-intensive and costly because phenotypes need to be measured in replicated field trials, in multiple environments, and over multiple seasons. This means that only single easy-to measure phenotypic traits are usually studied, which has created a bottleneck in breeding for these traits. To address this issue, scientists have developed non-destructive 'high-throughput phenotyping' (HTP) methods [18–20]. These methods allow significantly quicker measurement of more traits under field conditions as compared to traditional methods. The speed of data collection allows multiple screens which capture the whole-life cycle of the plants, not just at single time points. Advancements in sensor technology and statistical techniques have boosted progress in enabling high-throughput phenotyping for photosynthesis under field conditions [21–23]. These methods now offer alternatives for measuring photosynthetic traits that can rapidly cover field experiments involving several hundred accessions.

Genome-wide association studies (GWAS) are powerful tools for identifying associations between phenotypic traits and allelic variants across diverse varieties. Rice is particularly well-suited for GWAS due to its abundant natural variation and the extensive sequencing data available in the 3 K RG project. This approach has been widely applied in rice research to uncover genetic factors influencing agronomic traits

such as yield, stress tolerance, and metabolism [24–27]. Multiple quantitative trait loci (QTLs) associated with photosynthesis have been identified by GWAS, such as two QTLs associated with CO_2 assimilation rate located on chromosomes 4 and 8 in temperate japonica rice varieties [28]. Together with HTP approaches, GWAS offers an unprecedented ability to understand the genetic architecture of complex traits such as photosynthesis. Through the comparison of a diverse range of rice genomes, we can identify alleles present in rice grown across various environments to dissect the genetic foundation of key mechanisms in photosynthesis.

This study evaluated 318 lines representing the genetic diversity of indica rice for 45 traits, including photosynthetic traits, leaf anatomy traits, and agronomic traits, across three dry seasons. The correlations between these traits and rice yield were also investigated. We performed GWAS analyses to identify the co-location of photosynthetic traits with other traits. By examining a large indica rice panel over multiple years and exploring the relationship between photosynthetic capacity and yield, this study provided valuable insights that may accelerate molecular breeding for the development of high-yielding rice varieties.

2. Materials and methods

2.1. Plant growth conditions

Field experiments were conducted over three dry seasons (2016, 2017, 2019) at the International Rice Research Institute (IRRI) research farm in Los Baños, Laguna, Philippines (14° 08'55" N, 121 ° 15'49" E). In each of the three years, a total of 318 indica rice accessions were screened. These accessions were specifically chosen for their ability to flower at the IRRI research farm during the dry season. The plots were comprised of 5 × 6 hills with a single plant per hill and spacing of 20 cm between hills (Fig. 1). The field designs were partially replicated, and randomizations were performed independently for each year. The accession names and the corresponding replicates evaluated in each year are listed in Table S1. Twenty-one-day-old rice seedlings were transplanted on January 16, 2016; January 29, 2017; and January 31, 2019. At 7 days after transplanting (DAT), basal fertilizer was applied at a rate of 35–35–35 kg N–P–K ha^{-1} as a complete fertilizer. Urea was subsequently applied as the first topdressing at a rate of 150 kg ha^{-1} between 18 and 24 DAT. Additionally, ammonium sulfate at 10 kg ha^{-1} was applied 8 weeks after transplanting. The plants were maintained under favorable, irrigated conditions following IRRI's standard procedure. In the 2016 and 2017 experiments, potassium chloride was applied as the second topdressing at a rate of 50 kg ha^{-1}, also at 8 weeks after transplanting. The average temperatures during the 2016, 2017 and 2019 experiments were 28.25 °C, 27.5°C, 27.25°C, respectively. Correspondingly, the average humidity levels were 65.25%, 68.5% and 65.5% for the same years.

2.2. Trait data collection and processing

2.2.1. Leaf anatomy traits

Leaf anatomy traits were measured as per IRRI Genebank standards for rice [29]. Ligule length (LIGLT), leaf blade length (LLT), and leaf width (LWD) were measured manually at 10 weeks after transplanting. Ligule length was measured on 5 samples per accession from the base of the collar to the tip of the ligule of the penultimate leaf, i.e. the leaf below the flag leaf. Leaf width was measured at the widest portion of the penultimate leaf (i.e. highest leaf below the flag leaf) on the main culm on five representative plants. Flag leaf length (FLT) and width (FLWD) were manually measured on 5 representative plants per plot at 7 days after anthesis. Culm length (CULT) was measured from ground level to the base of the panicle on 5 plants per plot. Culm diameter (CUDI) was measured using a digital caliper. Culm number (CUNO) was recorded as the total number of grain-bearing and non-bearing tillers on 5 plants per plot. Panicle number per plant (PNO) was recorded as the total number of panicles on 5 plants. Panicle length (PLT) and the length of the main panicle axis were measured manually from the panicle base to the tip of 5 plants per plot at 7 days after anthesis or at full panicle exertion.

2.2.2. Leaf water potential-related traits

At booting stage in 2017 and 2019, leaves were sampled to determine the leaf water potential (LWP) by inserting one leaf into a pressure chamber at mid-day, pressurizing the leaf using compressed N_2 and recording the minimum pressure at which outward sap flux was observed. After LWP measurement, the leaves were immediately placed in a plastic bag with water and brought to the laboratory where they were fed into the LI-3100C Area Meter (LAM) connected to a laptop to automatically record leaf area (Area), leaf length, and maximum leaf width. Leaves were then oven-dried, and the specific leaf area (SLA) was calculated as the ratio of leaf area (Area) to leaf dry weight (Leaf_DW).

2.2.3. Photosynthesis-related traits

Gas exchange measurements were conducted between booting and flowering stages, specifically at 51 & 55 DAT in 2016, 53 & 57 DAT in 2017, and 46 & 50 DAT in DS2019. Five plants per plot were selected and tagged. The youngest fully expanded leaf or if the plant was in the booting stage, the penultimate leaf, was chosen for measurement. Instantaneous measurements of maximum photosynthesis (Photo, μmol CO_2 m^{-2} s^{-1}), stomatal conductance to water vapor (COND, mol H_2O m^{-2} s^{-1}), intercellular CO_2 concentration (Ci, mmol CO_2 mol^{-1}), water-use efficiency (WUE) and transpiration (TRMMOL, mmol H_2O mm^{-2} s^{-1}) were conducted under ambient conditions between 08:00 h and 13:00 h. Measurements were made using a portable photosynthesis system, LI6400XT (Li-Cor, Lincoln, NE USA) fitted with a standard 2 × 3 cm leaf chamber and a 6400–02B light source. Reference CO_2 was set to 400 μmol mol^{-1} and photosynthetic active radiation (PAR) was set at 1500 μmol photon m^{-2} s^{-1}. Leaf temperature for all measurements was maintained at 30 °C. The relative humidity of the chamber was maintained at 65–70% with a flow rate of 400 μmol s^{-1}. The leaf-to-air vapor pressure deficit (VPD) was kept between 1.5 and 2.5 kPa for all measurements. All of the data were recorded after achieving a steady state for all gas exchange parameters.

2.2.4. Agronomic traits

The days to heading (DTH) were recorded once 80% of the plants within the plot had flowered. Grain yield was taken from 12 hills per plot in 2016, 2017 and 2019. Grains were dried at 40 °C for three days and then dried for ~one month at 15%RH and 15 °C, then yield was calculated at a 14% moisture content. In 2017, the total above-ground biomass (biomass) from 12 hills per plot, which included panicles and straw, was collected, dried at 40°C for three days, and then weighed. The harvest index (HI) was determined by dividing the grain mass by the total above-ground biomass. The growth duration (GD) was recorded on the harvest day, while the grain filling duration (GFD) was the number of days between heading to harvesting.

2.2.5. Stomatal density measurement

The same segment of leaf that was used for the gas exchange measurement was tagged and collected a week after gas exchange measurements for stomatal measurement. Leaves were placed in labeled falcon tubes containing water. In the laboratory, the tip and base portion of the leaf were removed, and the middle segments were fixed in tubes containing formaldehyde-acetic acid-alcohol (FAA) solution under a fume hood. The tubes were then placed in racks and stored at room temperature until further processing. Clear abaxial epidermal peels were prepared by gently scraping away the mesophyll tissue with a sharp blade following the procedure of J. Chatterjee, et al. [30]. The underlying epidermal peels were mounted in water on glass slides and examined under a 400x magnification on Olympus BX51 and Olympus BX61 motorized microscope. Digital images were captured using an Olympus DP71 digital image documentation system on both

microscopes. Stomatal densities (SD) were determined from the entire field of view in each image. Numbers of stomata (s) and epidermal cells (e) were counted from the photomicrographs using ImageJ image processing software (Wayne Rasband, National Institute of Health, USA). The leaf stomatal index (SI) was estimated using the formula [s/(e + s)]× 100.

2.2.6. High throughput phenotyping traits

Drone imaging flights were conducted weekly from approximately 20 days after transplanting until harvest using a fixed wing sensefly eBee drone equipped with RGB (senseFly S.O.D.A.), multispectral (Parrot Sequoia) and thermal (senseFly ThermoMAP) cameras, in combination with a DJI Matrice M100 quadcopter equipped with RGB (DJI X3) and five-band multispectral (MicaSense RedEdge-M) cameras. A minimum of 6 ground control points located around the perimeter of the field were surveyed using RTK GPS (Leica Geospatial) and used during processing to georeference the imagery. Calibration panel images taken prior to each flight were used for radiometric calibration of multispectral imagery during processing. Imagery was processed using PIX4D Mapper Pro software with standard 3D mapping templates for RGB, multispectral and thermal imagery. Processing outputs included full resolution digital surface model (DSM) and index maps (WGS84 UTM 51 N coordinate system) for each camera band.

Rectangular polygon shapefile plot maps were generated using the fishnet tool in ArcMap and adjusted manually as needed to align with early season imagery. The polygons were reduced in size by 20 cm on all sides to eliminate edge effects. The plot sampling area of plots with missing rows was further reduced to include only the planted area. Plot level pixel data was extracted using R 3.2.2 [31] to calculate median plot values for each camera band and the values of normalized difference vegetation index (NDVI). Median values were used to reduce the influence of outliers associated with mixed pixels, shadows, soil background, and other noise sources common in UAV-derived field imagery. The calculations of NDVI and canopy temperature were conducted as described by Tanger et al. [20]. The pixel count and standard deviation for each camera band and a subset of indices was also computed for evaluation of plot variability. Canopy height was measured by drone in 2017 and 2019 and calculated as the difference between median plot DSM elevation and the pre-season mean plot DSM elevation. The data was compiled for the entire season into a single table in csv format. The NDVI was used to calculate the relative growth rate (RGR), which represents the difference between two time points just before the NDVI reached its peak, divided by the number of days between these two points. The relative senescence (SR) was calculated from the period before the end of NDVI measurements. The measurement periods of RGR and SR are indicated in Fig. 2.

The relative growth rate (RGR1) and the relative senescence rate (SR) were derived from the NDVI values.

$$RGR1 = \frac{In(NDVI_{D2}) - In(NDVI_{D1})}{(Day2 - Day1)}$$

$$SR = \frac{In(NDVI_{D1}) - In(NDVI_{D2})}{(Day2 - Day1)}$$

Where $NDVI_{D1}$ and $NDVI_{D2}$ are the NDVI values at two different time points, and *Day 1* and *Day 2* are the corresponding days.

The relative growth rate (RGR2) was derived from the HT values.

$$RGR2 = \frac{In(HT_{D2}) - In(HT_{D1})}{(Day2 - Day1)}$$

Where HT_{D1} and HT_{D2} are the HT values at two different time points, and *Day 1* and *Day 2* are the corresponding days. The measurement times for HT1 in 2016, 2017, and 2019 were 58, 50, and 48 DAT (days after transplanting), respectively, while for HT2 they were 87, 88, and 89 DAT, respectively.

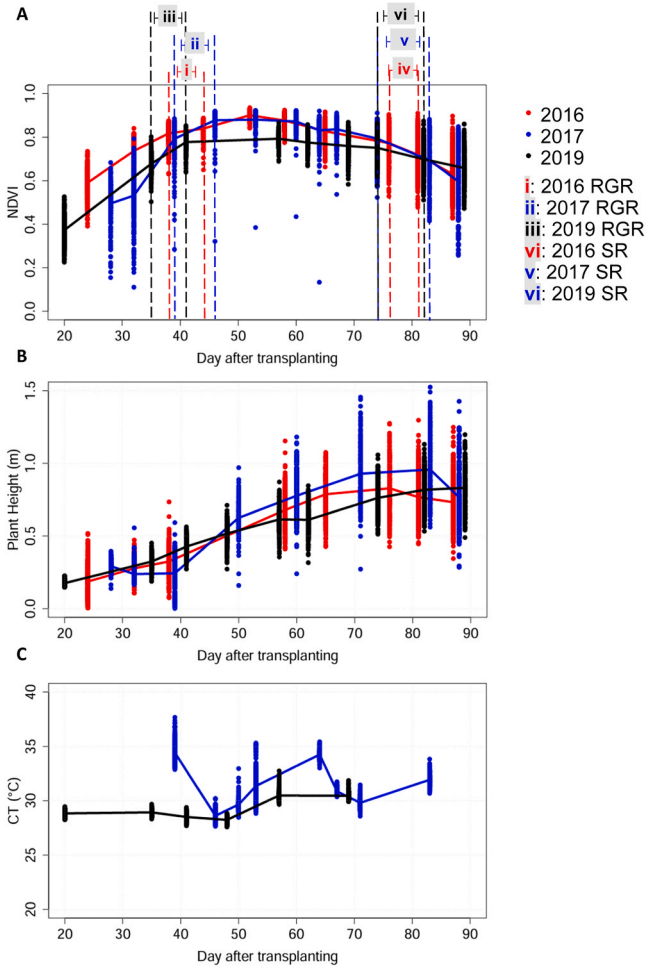

Fig. 2. Time course of HTP traits, (A) NDVI (B) plant height (C) canopy temperature, during the growing periods in 2016, 2017 and 2019. The data from 2016, 2017 and 2019 are presented in red, blue, and black. The solid lines are the means of all accession. i, ii, iii indicate the periods for calculating relative growth rate (RGR) in 2016, 2017 and 2019, respectively. iv, v, vi indicate the periods for calculating relative senescence rate (SR) in 2016, 2017 and 2019, respectively.

2.3. GWAS analysis

Genome-wide association (GWA) analysis was performed using genome-wide efficient mixed model analysis software (GEMMA v. 0.95 alpha) [32]. The 4.8 million single nucleotide polymorphisms (SNP) marker set downloaded from the Rice SNP-Seek database [33,34] was merged with imputed HDRA samples [35]. Then the target subset of samples was extracted and re-filtered for < 15% of missing data and minor allele frequency > 3% using PLINK 1.9 [36,37]. After removing highly correlated SNPs via LD (linkage disequilibrium) pruning with r^2 = 0.98 using the PLINK command "–indep-pairwise 15 kb 1 0.8", the final data set of 1008345 SNPs was used for GWAS. Additionally, we generated a second LD pruned dataset with more stringent criteria (r^2 = 0.6) for kinship and PCA calculation. The kinship matrix and principal components (PC) were computed using GEMMA command "-gk 1" and PLINK "–pca", respectively.

Mixed linear model (MLM) analysis with kinship matrix and principal components as fixed effect covariates was performed. The optimal number of principal components was determined by testing associations between PCs and phenotypes, and was set to 7 for most traits. Significance thresholds were calculated according to [38,39]. The estimated effective number of independent tests was 52,319, which corresponds,

Table 1
Significant correlations between photosynthetic rate (Photo), stomatal density (SD), and grain yield with other measured traits in 2016, 2017, and 2019. * indicates significant correlations (p-value <0.05). Background color indicates correlation strength: close to 1 in dark green, close to 0 in white, and close to −1 in dark red. Measurements that were not conducted in a given season are represented as NA with a gray background.

	Trait	2016	2017	2019
Photo vs	Cond	0.6205*	0.4836*	0.4063*
	Trmmol	0.5982*	0.4387*	0.5154*
	WUE	-0.0055	0.2112*	0.1548*
	SD	0.1744*	0.1034	0.2474*
	CULT	-0.256*	-0.0864	NA
	LLT	-0.2276*	-0.0776	NA
	Grain_Yield	0.0853	0.1539*	0.2055*
	BIOMASS	NA	0.1177*	NA
	DTH	-0.0069	0.112*	0.0668
SD vs	Cond	0.1636*	0.028	0.2436*
	Trmmol	0.1887*	-0.0412	0.1559*
	SI	NA	NA	0.1939*
	CUDI	0.2691*	0.1579*	NA
	CULT	-0.5783*	-0.2032*	NA
	CUNO	-0.0617	-0.2196*	NA
	LLT	-0.4024*	-0.1095	NA
	LWD	0.2361*	0.0325	NA
	PNO	NA	-0.2208*	NA
	FLLT	-0.1948*	NA	NA
	FLWD	0.1747*	NA	NA
	DTH	0.0442	0.2696*	0.1316*
	GD	NA	0.3081*	NA
	BIOMASS	NA	0.2825*	NA
	Grain_Yield	0.2833*	0.179*	0.1905*
	Area	NA	0.1888*	0.0209
	SLA	NA	0.0274	-0.1388*
	leaf.DW	NA	0.2545*	0.0879*
Grain Yield vs	Cond	0.086	0.1261*	0.1986*
	Trmmol	0.0401	0.1977*	0.1301*
	CUNO	-0.1521*	0.0191	NA
	CULT	-0.018	-0.257*	NA
	LIGLT	0.1686*	-0.02	NA
	LLT	0.1212*	-0.16*	NA
	LWD	0.2361*	0.0229	NA
	PLT	0.2723*	NA	NA
	FLLT	0.2368*	NA	NA
	FLWD	0.2692*	NA	NA
	DTH	0.2645*	0.0143	0.0539
	GFD	NA	-0.1254*	NA
	BIOMASS	NA	0.4403*	NA
	HI	NA	0.5796*	NA
	Average_Width	NA	0.1644*	0.1898*
	LWP	NA	0.0011	0.1272*

via a Bonferroni-Sidak style correction for nominal significance level alpha= 0.05, to a cutoff of −log10(p) at 6.01, which was taken as the conservative genome-wide significance level. In addition to this (still conservative) genome-wide significance threshold, to increase sensitivity we employed a suggestive threshold of -log10(p) = 5 as is common in rice GWAS studies. To determine GWAS peak (QTL) extent around each genome-wide significant SNP, we used LD clumping implemented in the PLINK "1.9 –clump" command (with settings r2 = 0.5 and p2 = 0.001). Overlapping LD clumps were merged to obtain a final list of QTLs. For haplotype analyses, SNPs in the region of identified loci

were downloaded from the Rice SNP-Seek Database (https://snp-seek.irri.org). Haplotype groups were defined by merging haplotypes with small genetic distance using hierarchical clustering in R. Association between haplotype groups and phenotypes was tested with the lm() function using both original phenotype values and residuals from population structure adjustment. The post-GWAS/QTL analysis was conducted to examine the QTLs associated with target traits and to provide insights into the potential functions of genes within the QTL regions. Coexpression network analysis was performed using RicePilaf with the RiceNet V2 dataset [40,41], and modules were detected using the ClusterOne algorithm [42].

2.4. Correlation analysis and three penalized regression models

Correlation analysis was performed in R 4.3.3 [43] using the package "corrplot" [44]. Additive main effects and multiplicative interactions (AMMI) analysis was conducted using agricolae package (v. 1.3.5) [45,46]. For prediction of photosynthetic traits from HTP indices (NDVI, HT for 2016 and NDVI, HT, CT for 2017, 2019), the plot-level values were averaged per genotype. Three penalized regression models were Lasso, Ridge Regression, and Elastic Net with mixing coefficient $\alpha = 0.5$ using R package "glmnet" [47]. For each model, the penalty parameter λ was optimized using a repeated 10-fold cross-validation procedure (2 repeats) using R package "tidymodels" and "tune" [48,49] across logarithmically spaced grid from $10^{-4.5}$ to $10^{1.3}$. The model minimizing the root mean square error (RMSE) averaged across the 20 assessment folds was selected.The predicted values across the 20 assessment folds were used to create scatterplots of predicted vs actual trait values.

3. Results

3.1. Variations and correlations of phenotypes

To investigate genetic variation in the relationships between rice photosynthesis, agronomy, leaf morphology, and indices collected by HTP, a panel of 318 indica accessions (Table S1) was evaluated during the dry seasons of 2016, 2017, and 2019. The exact numbers of accessions measured for each trait varied in different years due to time and labor constraints (Table S2). The average temperature in 2016 (28.3℃) was higher than in 2017 (27.5℃) and 2019 (27.3℃), and the humidity in 2017 (69.5%RH) was higher than in 2016 (65.3% RH) and 2019 (63.5% RH) (Fig. 1). Most of traits showed strong correlation coefficients across years, suggesting that genetics played a more significant role in controlling these traits than environmental factors (Table S3).

The photosynthetic traits exhibited significant correlations with each other in all three years (Table 1 and Figure S1). The photosynthetic rate (PHOTO) exhibited significantly positive correlations with stomatal conductance (COND) and transpiration rate (TRMMOL), while demonstrating a negative correlation with water use efficiency (WUE). In addition, the photosynthetic rate (PHOTO) was positively correlated with grain yield and biomass but negatively correlated with leaf blade length (LLT) and culm length (CULT). Stomatal density (SD) showed significant positive correlations with photosynthetic traits, including PHOTO, COND and TRMMOL and some agronomic traits that included Grain Yield, days to heading (DTH), growth duration (GD), and Biomass (Table 1; Tables S4-S6). Negative correlations were observed between stomatal density (SD) with leaf morphology and plant growth traits, including LLT, flag leaf length (FLLT), CULT, culm number (CUNO), and panicle number (PNO). Grain yield showed a strong positive correlation with harvest index (HI) and biomass, as well as positive correlations with several leaf and panicle morphology traits such as LWD, LIGLT, FLLT, FLWD, and PLT (Table 1). Days to heading (DTH) exhibited positive correlations with PHOTO, SD and grain yield (Table 1; Tables S4-S6). DTH also showed positive correlations with leaf and panicle morphology traits (LLT, LWD, LIGLT, FLLT, FLWD, CULT, PLT). On the other hand, grain filling duration (GFD) showed negative correlations with biomass and DTH.

The high throughput phenotyping (HTP) traits, including NDVI and plant height (HT), were collected across all three years, while canopy temperature (CT) data were only collected in 2017 and 2019 (Fig. 2). The NDVI values showed an increase until approximately 50 days after transplanting (DAT), while HT continued to increase until around 80 (DAT), and these trends were consistent across all three years. Additionally, canopy temperature exhibited relatively more stable values in 2019 compared to 2017. The correlation analysis across the growing period showed that NDVI values were negatively correlated with PHOTO, COND and Tmmol at early stages across the three years (Fig. 3). However, the correlation between NDVI and WUE varied across years: the correlations were positive for most time points in 2016, remained consistently but weakly positive in 2017, and were nearly absent in 2019 (Fig. 3). Days to heading (DTH) was positively correlated with NDVI at later growth stages when the NDVI was decreasing, and grain yield was positively correlated with NDVI at around 50–60 days after transplanting when the NDVI was highest (Figure S2). NDVI at the late growth period was positively correlated with leaf and panicle morphology traits (CULT and LLT), leaf blade length (LWD), panicle length (PLT), and FLLT, but negatively correlated with PNO and CUNO in 2016 and 2017 (Figure S2). The correlation analysis of the NDVI relative growth rate (RGR1) and NDVI relative senescence rate (SR) showed that DTH was positively correlated with RGR1, but negatively with SR in all three years. SR was highly correlated among the three years, but not for RGR1 (Table S7).

The canopy height (HT) drone-based measurements exhibited a high positive correlation with NDVI values measured on similar dates (Fig. 3; Tables S4-S6). The HT was also positively correlated with RGR2 and DTH. In addition, RGR2 was more strongly correlated with leaf morphology traits as compared with RGR1. RGR2 was significantly positively correlated with SD in 2017 and 2019. The canopy temperature (CT) was negatively correlated with NDVI, HT, COND, and grain yield, but positively correlative with DTH, GD, RGR1, RGR2, and PHOTO in the early growth period (Fig. 3; Tables S5-S6). In the late growth period (after 60 DAT), the CT was negatively correlated with PHOTO, COND, DTH, GD, BIOMASS, Grain Yield, NDVI, and HT, but positively correlated with SR (Table S8). CT was significantly negatively correlated with SD at most measurement times in both 2017 and 2019.

The principal component analysis (PCA) showed that traits with strong correlations clustered closely together (Figure S3). For example, PHOTO, Trmmol, and COND grouped tightly and were positioned near SD. NDVI measurements also formed two distinct clusters, separating early stage observations (before 50 DAT) from later stage measurements (after 60 DAT) consistently across all three experimental years. The AMMI biplots further revealed clear genotype × year interaction patterns across traits (Figure S4). PHOTO, COND, and Trmmol exhibited strong and similarly oriented interaction structures, indicating that gas exchange traits were highly responsive to interannual environmental variation, particularly in 2017 (Figure S4A–C). In contrast, WUE showed weak interactions, with most genotypes clustering near the origin, while SD displayed minimal G×E effects, as evidenced by tight genotype clustering along IPCA1 and short, similarly oriented year vectors (Figure S4D–E). Grain yield demonstrated the strongest G×E interactions among all traits, with broad genotype dispersion and clearly separated year vectors, reflecting the cumulative impact of environmental variation on final productivity (Figure S4F).

To test the predictive capacity of the HTP derived vegetative indices (NDVI, HT, CT) on five photosynthetic traits, we ran three penalized regression models: Lasso, Ridge Regression (RR), and Elastic Net (EN) for each trait-year combination. The EN model was set up with mixing coefficient alpha= 0.5 interpolating equally between RR and Lasso

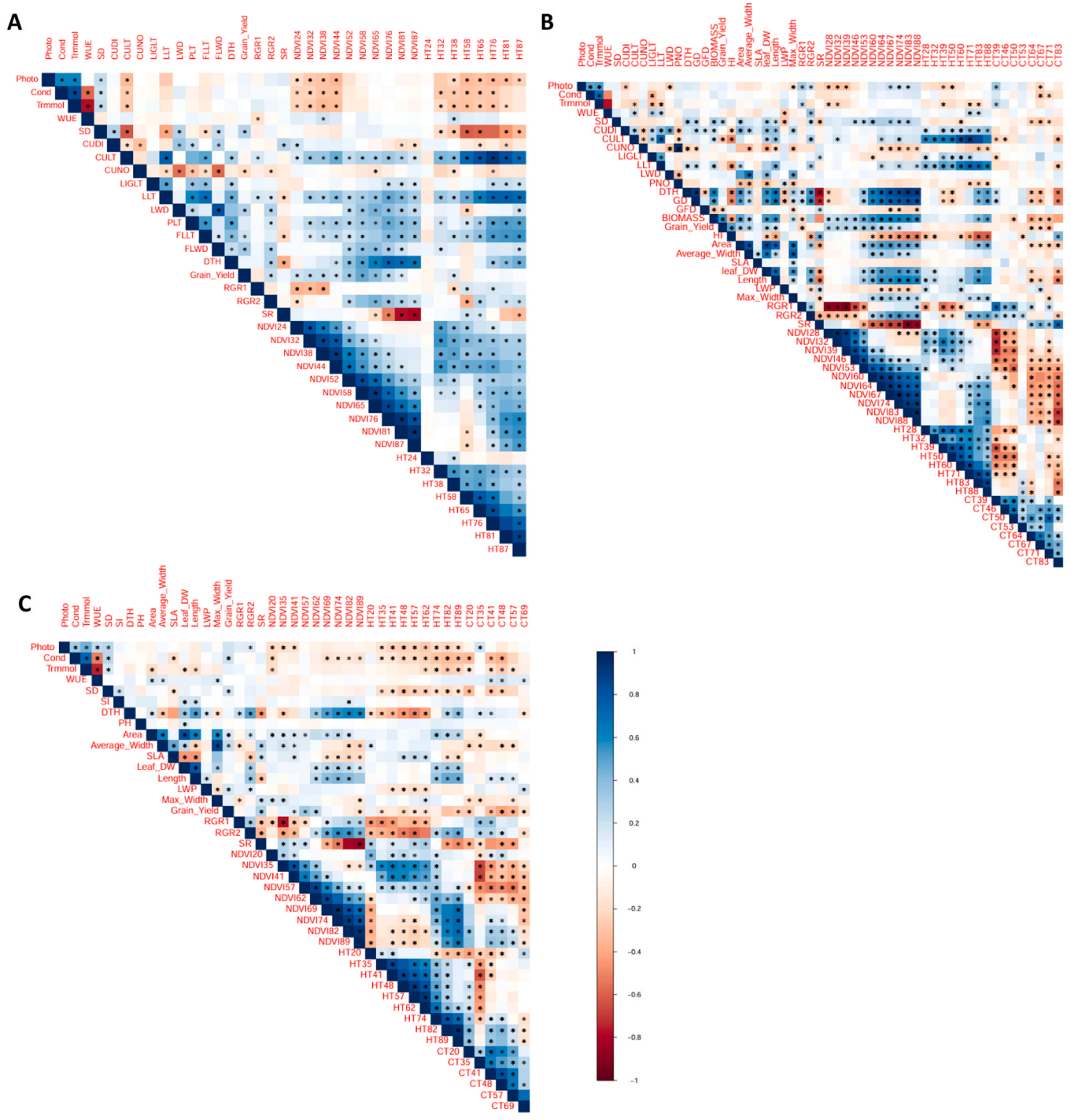

Fig. 3. Correlations plot of traits measured in (A) 2016, (B) 2017, and (C) 2019. The NDVI20-NDVI89 represent NDVI measured at 28–89 days after transplanting (DAT). HT and CT were measured at corresponding DAT intervals. The matrix displays colors indicating correlation strength and direction, with deep blue for strong positives and deep red for strong negatives. Significant correlations ($P < 0.05$) are marked with an asterisk (*); non-significant correlations are left blank. Correlations were calculated using pairwise complete observations. Traits include photosynthetic rate (Photo), stomatal conductance (Cond), transpiration rate (Trmmol), water use efficiency (WUE), stomatal density (SD), and stomatal index (SI).

penalties. Fig. 4 shows the average cross-validation R squared value for each year and trait, representing an estimate of predictive capacity on unseen data. Predictive capacity had a strong effect of year (2016 had higher R^2 values across traits compared to the other two years) and by trait, ranging from 7.3% (WUE 2019) to 44.3% (SD 2016). As for individual genotype predictions, the range of out-of-fold predicted values for SD was consistently narrower than that of observed values (Fig. S26). All three models reported similar average R^2 values with relatively little variation across years.

Seventeen accessions that were ranked in the Top 30 for photosynthetic rate in two or three years also exhibited correspondingly high stomatal conductance and transpiration rates (Table 2). Conversely, these same high-photosynthesis accessions demonstrated a trade-off in the form of diminished water use efficiencies. Several among those 17 accessions exhibited elevated stomatal densities and correspondingly achieved higher grain yield (Table 3). However, the plant height of these 17 accessions, whether measured manually (PH) or via drone measurements (HT), generally tended to be shorter (Table 3).

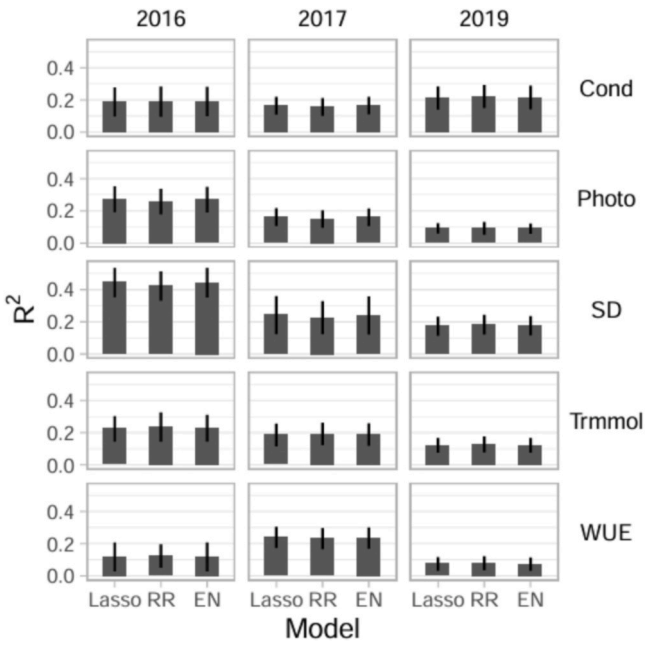

Fig. 4. Cross-validation R squared of the 3 penalized regression models (Lasso, Ridge Regression (RR), Elastic Net (EN)).

3.2. GWAS analysis

The diverse range of phenotypic traits in this indica panel presents a valuable opportunity for performing a genome-wide association study (GWAS) aimed at identifying genetic markers linked to multiple traits. The panel contains accessions from all 4 indica subgroups defined in Wang et al. (2018) at K= 9, representing a subset of global indica variation. The first two principal components effectively separate the known subgroups (ind1A, ind1B, and ind2), while also revealing the prevalence of admixed individuals within the indica group. These

Table 2
Photosynthetic trait values (ranked in brackets) for 17 selected accessions. These 17 accessions ranked in the top 30 for at least 2 out of 3 years for photosynthetic rate (Photo). NA: No Data.

	Trait	Photo	Photo	Photo	Cond	Cond	Cond	Trmmol	Trmmol	Trmmol	WUE	WUE	WUE
Accession	Year	2016	2017	2019	2016	2017	2019	2016	2017	2019	2016	2017	2019
ARIANA::GERVEX 396-C1		NA	34.9 (3)	35.6 (9)	NA	1.05 (94)	1.52 (4)	NA	12.3 (85)	16.9 (2)	NA	2.83 (45)	2.10 (306)
C 662083::IRGC 62101–1		25.0 (13)	29.8 (27)	34.5 (10)	0.85 (77)	1.30 (25)	0.87 (113)	9.6 (117)	12.6 (76)	12.2 (49)	2.61 (13)	2.36 (156)	2.81 (131)
CN 44–40–7::IRGC 45368–1		24.84 (15)	22 (264)	33.3 (21)	1.17 (14)	1 (113)	0.98 (58)	14.7 (3)	12 (96)	11.9 (65)	1.69 (178)	1.83 (282)	2.81 (132)
CT 9506–18–7-1T-2::IRGC 116973–1		26.0 (7)	30.7 (17)	34.3 (10)	0.83 (83)	0.67 (288)	0.94 (77)	10.1 (99)	8.3 (290)	13.1 (29)	2.58 (17)	3.7 (2)	2.65 (174)
DA GANG ZHAN::IRGC 67103–1		NA	30.1 (23)	33.2 (21)	NA	1.08 (85)	0.68 (216)	NA	11.3 (126)	10.4 (160)	NA	2.67 (72)	3.19 (57)
FACAGRO 64::IRGC 82059–1		30.1 (1)	31.2 (11)	30.9 (69)	1.23 (9)	0.83 (199)	0.72 (197)	13.9 (7)	11.4 (123)	12.0 (61)	2.17 (89)	2.73 (64)	2.57 (204)
IR 19058–107–1::IRGC 72997–1		27.3 (3)	31 (15)	32.3 (35)	1.06 (36)	0.97 (132)	1.00 (54)	12.8 (20)	14.6 (23)	13.8 (15)	2.13 (99)	2.13 (220)	2.34 (269)
IR 77298–14–1–2–10::G1		26.2 (6)	30.6 (18)	28 (171)	1.07 (35)	1.09 (81)	1.37 (4)	12.6 (25)	13.8 (39)	13.4 (18)	2.24 (71)	2.21 (193)	2.24 (284)
IRGA 411–1–6-1F-A::IRGC 117344–1		24.0 (27)	31.2 (12)	34.2 (10)	1.21 (12)	1.21 (40)	1.23 (11)	13.3 (19)	13.6 (49)	13.5 (16)	1.81 (158)	2.29 (180)	2.52 (213)
J 6 IR 520 (WC 693)::IRGC 57600–1		24.3 (22)	25.6 (137)	33.1 (22)	1.03 (41)	0.67 (286)	0.96 (64)	11.5 (46)	9.8 (216)	11.6 (78)	2.10 (104)	2.62 (78)	2.85 (120)
KH 998::IRGC 16948–2		23.9 (30)	30.6 (21)	28.3 (159)	1.37 (3)	1.81 (1)	1.76 (1)	13.8 (8)	15.5 (14)	14.9 (9)	1.74 (171)	1.97 (246)	1.92 (303)
MALAGASY::IRGC 69717–1		24.8 (17)	30.4 (22)	29.0 (127)	1.15 (20)	0.92 (161)	0.95 (64)	13.7 (10)	10.4 (168)	12.3 (43)	1.81 (160)	2.92 (31)	2.37 (258)
SACHI::IRGC 46612–2		21.8 (94)	29.6 (29)	35.3 (9)	1.04 (38)	1.27 (27)	0.74 (178)	12.0 (36)	12.4 (80)	10.2 (166)	1.82 (157)	2.39 (149)	3.46 (26)
WAS 173-B-B-6–2–2::C1		26.7 (5)	31.1 (13)	31.5 (44)	1.08 (31)	1.01 (108)	1.11 (25)	12.0 (34)	17.9 (1)	12.1 (52)	2.24 (69)	1.74 (297)	2.60 (189)
WAS 21-B-B-20–4–3–3::C1		24.8 (16)	26.2 (113)	33.4 (16)	0.73 (127)	0.56 (317)	1.10 (28)	11.4 (51)	8.6 (278)	12.1 (50)	2.18 (87)	3.03 (25)	2.77 (135)
WAS 174-B-3–5::C1		24.6 (18)	30.8 (16)	32.3 (31)	0.88 (65)	1.2 (44)	0.87 (102)	10.9 (61)	14.2 (30)	9.7 (191)	2.25 (63)	2.17 (209)	3.32 (44)
WAS 199-B-1–2–1::C1		22.7 (61)	32.9 (6)	33.5 (13)	0.84 (82)	0.94 (146)	1.09 (28)	10.5 (75)	11.7 (114)	16.4 (2)	2.16 (93)	2.82 (52)	2.04 (295)

Table 3
Stomatal and agronomy traits (ranked in brackets) for 17 Selected accessions. These 17 accessions ranked in the top 30 for at least 2 out of 3 years for photosynthetic rate. NA: No Data.

Accession	Trait Year	SD 2016	SD 2017	SD 2019	SI 2019	BIOMASS 2017	Grain_Yield 2016	Grain_Yield 2017	Grain_Yield 2019	PH 2019
ARIANA::GERVEX 396-C1		NA	NA	NA	NA	1371.4 (38)	384.2 (168)	457.5 (87)	336 (66)	124.2 (77)
C 662083::IRGC 62101–1		626.9 (29)	515.3 (38)	NA	NA	897 (233)	399.8 (154)	413.9 (134)	126.8 (267)	120.3 (100)
CN 44–40–7::IRGC 45368–1		595.2 (53)	497 (48)	527.0 (42)	0.28 (231)	622.5 (304)	337.5 (231)	NA	280.2 (110)	77.5 (288)
CT 9506–18–7-1T-2::IRGC 116973–1		615.6 (35)	NA	424.7 (184)	0.29 (204)	1139.4 (114)	411.9 (139)	516.7 (32)	236.7 (159)	95.2 (214)
DA GANG ZHAN::IRGC 67103–1		NA	NA	458.0 (134)	0.32 (108)	1029.4 (163)	322.0 (243)	337.2 (219)	271.7 (120)	74 (300)
FACAGRO 64::IRGC 82059–1		421.5 (176)	448.3 (86)	467.4 (119)	0.31 (141)	996.3 (184)	308.3 (253)	351.1 (206)	87.2 (292)	96 (213)
IR 19058–107–1::IRGC 72997–1		533.9 (96)	528.4 (35)	544.0 (31)	0.29 (206)	1045.7 (153)	442.7 (94)	525.8 (30)	599.5 (1)	100 (203)
IR 77298–14–1–2–10::G1		565.3 (74)	287.3 (164)	488.3 (80)	0.29 (217)	1284.8 (49)	371.6 (187)	541.8 (22)	274.3 (117)	108.8 (161)
IRGA 411–1–6-1F-A::IRGC 117344–1		625.4 (31)	NA	495.0 (68)	0.34 (40)	1056.3 (151)	406.7 (149)	496 (49)	241.3 (153)	103.7 (183)
J 6 IR 520 (WC 693)::IRGC 57600–1		622.1 (33)	NA	NA	NA	1005.5 (179)	403.5 (151)	486.1 (57)	280.4 (108)	87.1 (245)
KH 998::IRGC 16948–2		696.9 (7)	470.7 (65)	616.4 (3)	0.28 (225)	1498.6 (17)	343.5 (225)	594.5 (11)	280.4 (109)	116.1 (125)
MALAGASY::IRGC 69717–1		573.3 (68)	NA	NA	NA	883.6 (239)	559.1 (15)	266.4 (275)	80.6 (296)	107 (173)
SACHI::IRGC 46612–2		487.5 (126)	447 (88)	491.0 (70)	0.32 (107)	1241.5 (64)	353.6 (215)	505.4 (45)	284.4 (105)	81 (278)
WAS 173-B-B-6–2–2::C1		579.4 (64)	534 (30)	572.0 (11)	0.37 (5)	1238 (67)	464.5 (72)	466.4 (77)	321.1 (77)	107 (134)
WAS 21-B-B-20–4–3–3::C1		602.8 (47)	521.1 (36)	NA	NA	1174.8 (97)	498.9 (47)	518.4 (31)	430.2 (12)	111.8 (147)
WAS 174-B-3–5::C1		603.3 (46)	638.5 (2)	NA	NA	1221.3 (73)	440.1 (69)	537.5 (25)	505.1 (4)	135.5 (28)
WAS 199-B-1–2–1::C1		763.6 (1)	608.2 (8)	478.2 (93)	0.35 (32)	1374.3 (37)	473.1 (93)	655.4 (4)	378.9 (33)	56 (247)

admixed accessions, labeled as "indx", occupy intermediate positions between the main indica subgroups on the PCA plot, reflecting their mixed genetic backgrounds (Figure S5). Significantly associated SNPs, indicated by a threshold of -$\log_{10}$ (P) > 5 and deviation from the expected values of -$\log_{10}$ (P) in the quantile-quantile plots (Q-Q), are considered to be associated with the traits (Figures S6-S25). QTLs were defined based on adjacent significantly associated SNPs within one estimated linkage disequilibrium (LD) block. The numbers of QTLs on each chromosome for each trait in the three years are listed in Table S9.

The majority of QTLs linked to photosynthetic traits were identified in a single year, with the exception of qTRMMOL-2–2 on Chr2 at 29.42–29.6 Mb, which was observed in both 2017 and 2019 (Table 4; Fig. 5). To identify recombinant genotypes of the photosynthesis-related QTLs and narrow down the list of loci of interest, we analyzed haplotype variation based on non-synonymous SNPs within the coding sequences (CDS) of non-transposable element (non-TE) genes located in the QTL regions. One candidate gene, LOC_Os02g48210, encoding a lectin-like protein kinase, was identified at qTRMMOL-2–2 as having three haplotypes with variation in transpiration rate (TRMMOL) (Fig. 6). In the 2017 data, Haplotype 1 (n = 41) was associated with a lower TRMMOL. Another candidate gene, LOC_Os04g32920, encoding a potassium transporter, was identified at qTRMMOL-4–1 as having two haplotypes associated (Fig. 7). In the 2016 data, Haplotype 1 (n = 176) was associated with lower transpiration rates compared to Haplotype 2 (n = 11). Among the 19 PHOTO QTLs, qPHOTO-1–2 (on Chr1 from 14.61 to 15.1) was found to contain haplotypes associated with variation in photosynthetic rate within the gene region of LOC_Os01g26210, which encodes an OsWAK receptor-like protein kinase (OsWAK6). Haplotype 1 (n = 156) was associated with a lower photosynthetic rate, while Haplotype 2 (n = 47), which carries a missense SNP, was associated with a higher photosynthetic rate (Fig. 8). The haplotype analysis of qPHOTO-associated QTLs showed that many of the 17 high-photosynthesis accessions belonged to haplotype groups associated with higher photosynthetic performance across multiple qPHOTO loci (Fig. 9).

The NDVI relative growth rates (RGR1) in 2017 exhibited the highest number of QTLs, totaling 44 (Table S9). The QTLs qRGR1–11–2 and qSR-1–1 were also detected in both 2016 and 2017 (Table S10). Stomatal density (SD) had only a few QTLs, including one QTL in 2016 and four QTLs in 2019, while no QTLs were detected in 2017. The most significant SNPs (-$\log_{10}$ (P) > 10) were found for the traits 2016 CULT, 2019 DTH, and 2016 LSEN. The QTLs for CULT detected in both 2016 and 2017 were qCULT-1–2, qCULT-1–4, qCULT-1–5, qCULT-1–6, qCULT-3–1, and qCULT-11–2. The QTL of qLLT-4–1 was detected on Chr 4 at 15.8–16.0 Mb in both 2016 and 2017. The QTLs for DTH detected in both 2016 and 2019 included qDTH-1–4 and qDTH-4–1 (Table S10). GWAS analysis for plant height measured by drone was conducted at two time points: one at the middle of the growing stage (HT1) and another at the end of the growing stage (HT2). Several QTLs for HT2 were simultaneously detected, including qHT2–1–3 and qHT2–1–4 for all three years, qHT2–1–6 for 2016 and 2017, and qHT2–7–2 for 2017 and 2019 (Table S10). The canopy temperature (CT) measured by drone at 50 and 48 DAT was used for GWAS analysis in 2017 and 2019, respectively. QTLs for CT didn't co-locate between the two years.

Many QTL regions co-located for different traits (Table S11). The regions of QTLs for different photosynthetic traits overlapped, such as qWUE-2–1/ qTRMMOL-2–1/qTRMMOL-2–2, qCOND-3–1/qTRMMOL-3–1, and qPHOTO-4–1/qCOND-4–2/qTRMMOL-4–1. The regions of qPHOTO-11–4/ qSR-11–1 also co-located at 23 Mb on Chr11 (Table S11). Furthermore, the QTL regions for several leaf and panicle morphology traits overlapped, including qCUNO and qPNO (qCUNO-1–1/PNO-1–1, qCUNO-2–1/qPNO-2–1, qCUNO-5–1/qPNO-5–1, qCUNO-9–1/qPNO-9–1, qCUNO-12–1/qPNO-12–1), qCULT and qLLT (qCULT-1–6/qLLT-1–1, qCULT-1–9/qLLT-1–2, qCULT-1–10/qLLT-1–3), qFLLT&qLLT F(qFLLT-5–1/qLLT-5–1, qFLLT-7–2/qLLT-7–6/qFLLT-7–3), qFLWD and qLWD (qFLWD-4–1/qLWD-4–1, qFLWD-12–1&qLWD-12–1), and qLLT and qCUNO (qLLT-7–4/qCUNO-7–4, qLLT-7–2/qCUNO-7–3& qLLT-7–3/qCUNO-7–4, qLLT-7–4/qCUNO-7–4/qLLT-7–5). The QTL regions for qSD-1–2 overlapped with the QTL for canopy temperature (qCT-1–3) and other HTP traits (qHT1–1–1, qHT1–1–2,

Table 4
The QTL detected in the GWAS analysis for photosynthetic traits and candidate genes.

Trait	QTL	Year	CHR	Peak SNP	Interval (Mb)	No. of SNPs	P-value of peak SNP	Candidate genes
Photo	qPHOTO-1–1	2016	1	12366132_A_G	12.3–12.4	50	2.55E-06	CRS2
	qPHOTO-1–2	2016	1	14856712_G_A	14.61–15.1	104	3.74E-06	OsRboh, OsWAK5–9, OsRLCK35, OsPDH
	qPHOTO-1–3	2016	1	16262685_C_T	15.77–16.74	229	1.11E-06	
	qPHOTO-1–4	2016	1	17338618_C_T	17.1–17.59	225	5.82E-06	EDM2, PSB01
	qPHOTO-1–5	2016	1	17921664_C_A	17.67–18.15	164	7.48E-06	LOC_Os01g32780
	qPHOTO-2–1	2017	2	2034633_C_T	2.03–2.04	8	1.46E-07	
	qPHOTO-3–1	2016	3	6062135_A_T	6.06–6.07	8	1.83E-06	
	qPHOTO-3–2	2016	3	27203929_A_C	27.16–27.21	7	6.09E-06	
	qPHOTO-4–1	2016	4	19877800_T_C	19.76–19.88	3	8.06E-06	
	qPHOTO-4–2	2017	4	31904961_G_C	31.9–31.9	1	6.07E-06	
	qPHOTO-6–1	2016	6	18371798_C_T	18.37–18.37	1	5.40E-06	
	qPHOTO-11–1	2016	11	8055672_C_T	7.89–8.2	32	8.78E-06	
	qPHOTO-11–2	2016	11	8472248_A_T	8.22–8.61	6	8.08E-06	
	qPHOTO-11–3	2017	11	19011314_G_A	18.77–19.26	164	1.86E-06	
	qPHOTO-11–4	2016	11	23138391_C_T	23.07–23.25	64	9.08E-07	
	qPHOTO-12–1	2019	12	21246404_G_A	21.1–21.45	4	1.46E-06	
	qPHOTO-12–2	2019	12	21599413_G_A	21.52–21.65	4	2.38E-06	OsAPRL6
	qPHOTO-12–3	2019	12	21751486_G_A	21.67–21.76	31	6.51E-07	
	qPHOTO-12–4	2016	12	21904870_G_A	21.82–21.91	17	7.51E-06	
Cond	qCOND-1–1	2017	1	31957100_C_T	31.71–32.2	82	1.36E-06	
	qCOND-2–1	2019	2	32339094_C_T	32.34–32.34	2	1.15E-06	
	qCOND-2–2	2019	2	32373789_A_G	32.37–32.37	1	9.62E-08	
	qCOND-3–1	2016	3	4421723_T_A	4.4–4.42	6	3.44E-07	
	qCOND-4–1	2019	4	12290635_G_A	12.08–12.54	203	7.73E-06	
	qCOND-4–2	2016	4	19912440_A_G	19.83–19.96	55	1.80E-06	
	qCOND-4–3	2016	4	20220278_A_G	19.98–20.33	461	4.06E-08	$qS_{ada}4.2$; $qS_{aba}4.2$ [50]
	qCOND-9–1	2016	9	15510718_A_G	15.5–15.53	3	8.96E-07	CSLC2
WUE	qWUE-2–1	2019	2	29412839_T_C	29.31–29.48	148	1.47E-06	
	qWUE-5–1	2017	5	19326508_A_G	19.15–19.33	5	9.26E-06	
	qWUE-8–1	2019	8	20948303_C_T	20.95–20.98	4	2.29E-06	
	qWUE-11–1	2016	11	23943110_G_T	23.71–24.12	29	4.61E-06	
Trmmol	qTRMMOL-2–1	2017	2	29142119_C_T	29.14–29.27	10	9.17E-06	OsMDHAR4
	qTRMMOL-2–2	2017	2	29427275_C_T	29.42–29.6	23	3.91E-07	OsPFP1α1
	qTRMMOL-2–2	2019	2	29477881_A_T	29.41–29.51	42	5.13E-06	
	qTRMMOL-3–1	2016	3	4421723_T_A	4.4–4.44	15	1.08E-07	
	qTRMMOL-3–2	2017	3	15114456_G_A	14.99–15.21	5	5.48E-06	
	qTRMMOL-4–1	2016	4	19912440_A_G	19.84–20.36	520	5.36E-07	OsHAK1
	qTRMMOL-4–2	2016	4	20886714_C_T	20.74–20.89	3	3.34E-06	
	qTRMMOL-9–1	2016	9	20596686_C_T	20.59–20.71	36	5.95E-06	
	qTRMMOL-12–1	2017	12	16504332_T_C	16.49–16.54	48	9.11E-06	

qHT2–1–2, qRGR1–1–3, qDTH-1–1) at 32.3–34.8 Mb on Chr1. The QTLs for SI overlapped with QTLs for RGR on Chr4 (qRGR1–4–5/qSI-4–1), and QTL for Leaf DW on Chr7 (qSI-7–2/qLeaf_DW7–1). Multiple QTLs overlapped within specific genomic regions, including 37.1–38.1 Mb (qDTH, qCULT, qRGR, qHT1) and 38.2–39.6 Mb (qDTH, qCULT, qHT1, qLLT, qHT2, qSD) on Chr1, and 0.3–0.6 Mb (qCT, qRGR, qHI) and 15.8–16.0 Mb (qDTH, qHI, qHT2, qLLT, qLeaf_DW, qCULT, qPLT) on Chr4.

Coexpression network analysis was performed to examine the potential functions of genes within the QTL regions of each chromosome using RicePilaf. One region with multiple overlapping QTLs on Chr1 38.2–39.6 (qDTH, qCULT, qHT1, qLLT, qHT2, qSD) was found in three gene modules to be significantly enriched. Two of these modules were enriched in gene ontology categories related to nitrogen utilization, indicating a potential functional link between this genomic region and nitrogen metabolism. For the region of qPHOTO-11–4/ qSR-11–1 on Chr11 23.0–23.2 Mb, it was found that out of 2608 total network modules evaluated, 10 modules were significantly enriched (adjusted p-value < 0.05) with genes from this QTL region. The most significantly enriched module (Module 1423) was annotated with the Trait Ontology (TO) term "abiotic stress." This module comprised six genes, including one gene previously implicated by GWAS/QTL analyses. The second most enriched module was also associated with "abiotic stress" and additionally enriched in the KEGG pathway "Sphingolipid metabolism," suggesting possible links to stress adaptation mechanisms. The third enriched module was characterized by the gene ontology term "ADP binding," primarily driven by the presence of the gene LOC_Os03g38240 within the module. The fourth module showed enrichment in KEGG pathways related to "MAPK signaling pathway," "Plant hormone signal transduction," and "Plant-pathogen interaction," suggesting broader roles in stress and defense responses. Additionally, the sixth module contained LOC_Os11g39000, encoding the transcription factor ILI2, and was enriched in KEGG pathways including "Starch and sucrose metabolism," "Steroid biosynthesis," and "Plant-pathogen interaction." These findings indicate that this QTL region on chromosome 11 may be involved in multiple stress response and metabolic processes, including abiotic stress tolerance, lipid signaling, hormone regulation, and pathogen defense.

4. Discussion

Understanding natural variation in photosynthetic capacity and its associated traits is essential for advancing rice improvement under increasingly variable climates. Across three field seasons, we observed substantial phenotypic diversity within an indica diversity panel, spanning photosynthetic, stomatal, morphological, and agronomic traits. For example, stomatal conductance varied three- to fivefold among accessions, while leaf photosynthesis rates showed less variation (Table S2). While these results validate the approach of using diversity panels to mine natural variation in photosynthesis, they also highlight the challenge of dissecting its underlying physiology. The relatively weak correlation between leaf photosynthesis rates and most anatomical and functional traits measured in our study underscores the complexity of photosynthesis as a dynamic trait which depends on interactions among multiple functional, anatomical, and biochemical traits, as well as trait-trait interactions and environmental influences (Tables S4-S6).

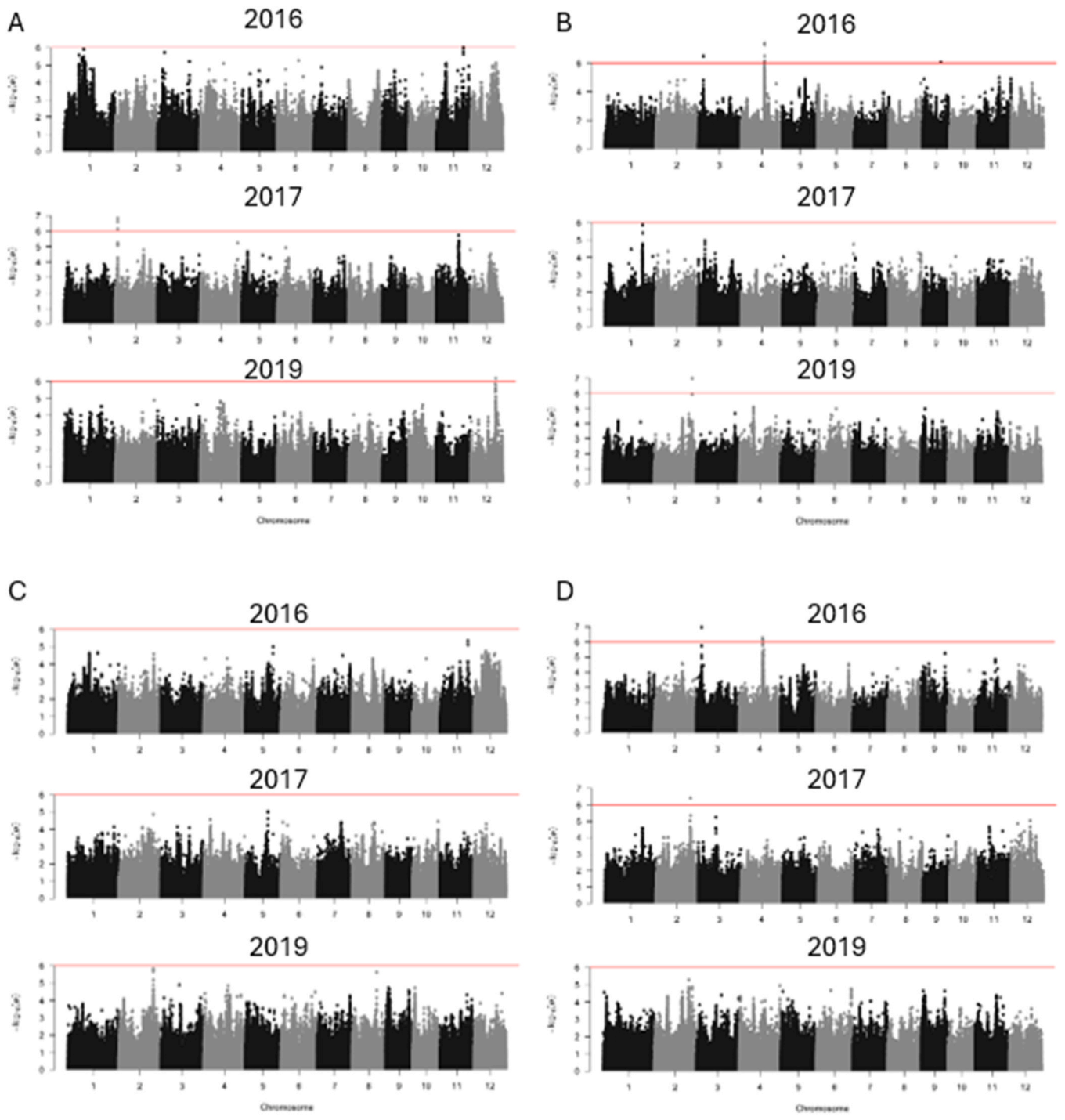

Fig. 5. Manhattan plots of GWAS results for photosynthetic traits in three years. (A) instantaneous measurements of maximum photosynthesis (Photo). (B) stomatal conductance to water vapor (Cond). (C) water-use efficiency (WUE). (D) transpiration (Trmmol).

The limited number of QTLs consistently detected across environments likely reflects the strong environmental sensitivity and phenotypic plasticity of photosynthesis-related traits under field conditions, rather than insufficient statistical power. Year-to-year variation in climate and phenology, together with partially replicated field trials, reduces the likelihood of identifying stable QTLs across environments, such that only a small subset—such as qTRMMOL-2–2—represents genetically stable loci. Given this complexity, integrating genetic analyses with physiological phenotyping provides a more informative framework for dissecting variation in photosynthetic performance. By combining haplotype analysis with multi-year field phenotyping, we identified accessions that consistently performed well across multiple photosynthesis-related loci. In particular, FACAGRO 64, a heat-tolerant indica line [51], carried favorable haplotypes at all qPHOTO regions (Fig. 9), highlighting it as a potential donor for improving photosynthetic efficiency. These results suggest that the genetic determinants of photosynthesis are partly conserved across environments, enabling the identification of elite haplotypes with broad breeding utility.

Our study also provides evidence addressing the long-standing discussion over whether leaf-level photosynthesis rates are associated with grain yields [3,11,52]. Previous studies have also found that rice photosynthesis positively correlates with grain yield and biomass, and

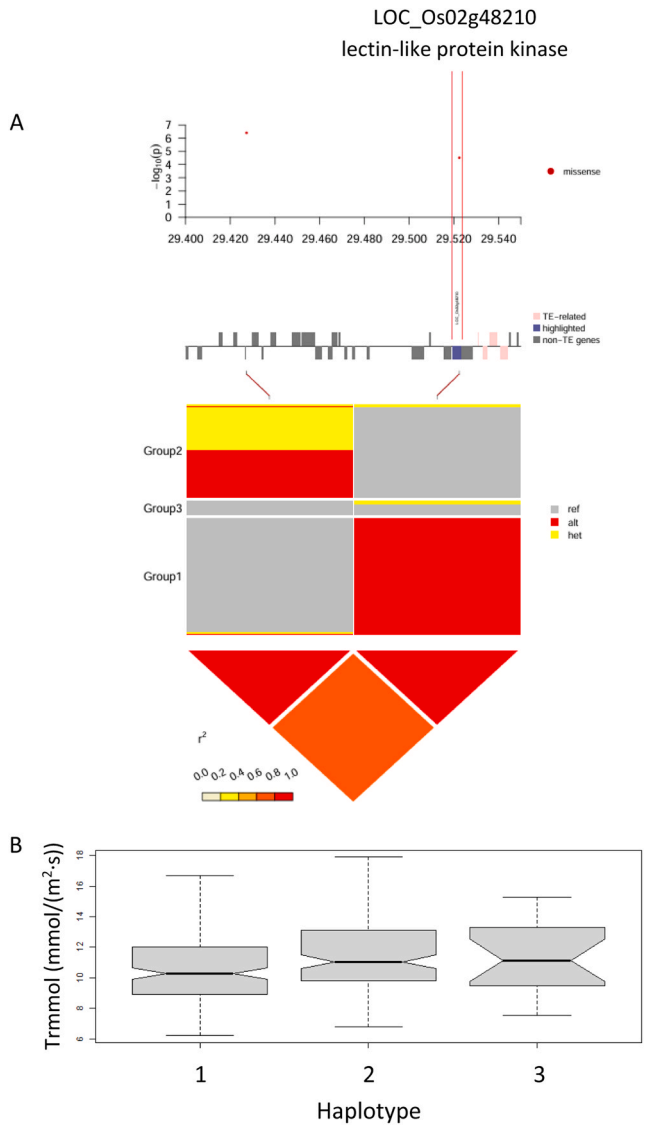

Fig. 6. Haplotype analyses of the LOC_Os02g48210 candidate gene at qTRMMOL-2–2. (A) Linkage disequilibrium (LD) block surrounding the region of LOC_Os02g48210 gene at qTRMMOL-2–2. (B) Boxplots for transpiration rate (Trmmol) 2016 based on haplotypes for qTRMMOL-2–2.

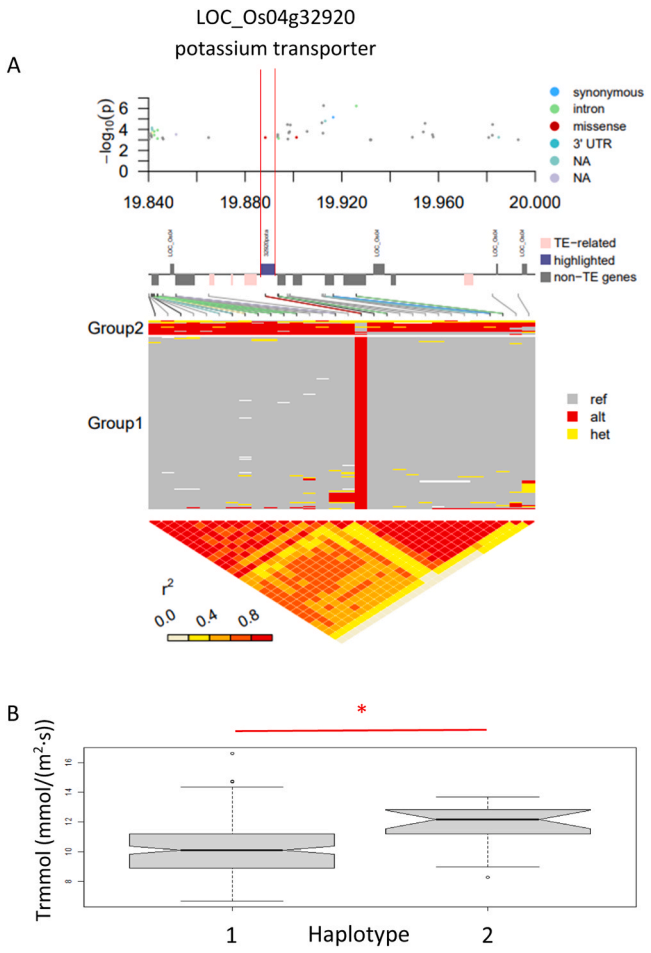

Fig. 7. Haplotype analyses of the LOC_Os04g32920 candidate gene at qTRMMOL-4–1. (A) Linkage disequilibrium (LD) block surrounding the region of LOC_Os04g32920 gene at qTRMMOL-4–1. (B) Boxplots for transpiration rate (Trmmol) 2016 based on haplotypes for LOC_Os04g32920. * indicates the level of significant different (T-test, $P < 0.05$) between the groups. (C) The SNP positions and alleles, the number of accessions and mean value of transpiration (Trmmol) for each haplotype.

several QTLs associated with leaf photosynthetic rate have been identified [3,53–55]. Consistent with these findings, our multi-trait, multi-year dataset showed robust positive correlations between photosynthetic rate, stomatal conductance, transpiration rate, water use efficiency, stomatal density, biomass, and grain yield (Table 1). Accessions with higher photosynthetic capacity generally exhibited greater gas-exchange activity and increased grain production. Positive correlations between stomatal density (SD) and grain yield further supports the conclusion that higher SD was associated with increased stomatal conductance, higher photosynthetic rates, and improved yield. Previous studies have also reported that stomatal conductance was positively correlated with SD and yield [13,56,57], as was in this study. Our results also showed that SD was negatively correlated with plant height, leaf length, and culm length (Fig. 3), suggesting that accessions with higher stomatal density may exhibit reduced vegetative growth and more compact plant architecture. These results were confirmed in several accessions which consistently ranked in the top 30 for photosynthetic rate over two or more years; they also showed elevated stomatal densities and produced higher grain yields but tended to have shorter plant height (Table 2). This supports the idea that modifying stomatal traits could influence both physiological efficiency and plant architecture.

The contrasting performance of some accessions across years illustrates the importance of environmental modulation of stomatal and photosynthetic traits. For example, CT 9506–18–7–1T-2 maintained high photosynthetic rates across seasons but displayed year-dependent variation in water-use efficiency, likely reflecting differences in SD and evaporative demand (Table 2 &3). AMMI analysis further showed that stomatal density remained remarkably stable across the three years and exhibited minimal genotype × year interaction, which is consistent with its largely genetically determined nature (Figure S4E). This stability of stomatal density across years makes it a promising target for genetic manipulation in the development of climate-resilient rice varieties. For instance, transgenic reduction of stomatal density in the rice cultivar 'IR64' has been shown to improve drought tolerance without compromising grain yield [58,59]. Other stomatal characteristics, including guard cell size, pore aperture, and the speed of stomatal opening and closing, may also serve as important targets for improving productivity and warrant further investigation.

Several QTLs for photosynthetic and stomatal phenotypes identified in our GWAS analysis have been reported as photosynthetic related markers or genes. For example, qPHOTO-1–2, which contains a photoassimilate defective gene (*LOC_Os01g26920*), and its mutant showed decreased carbon assimilate and yield production [60], and

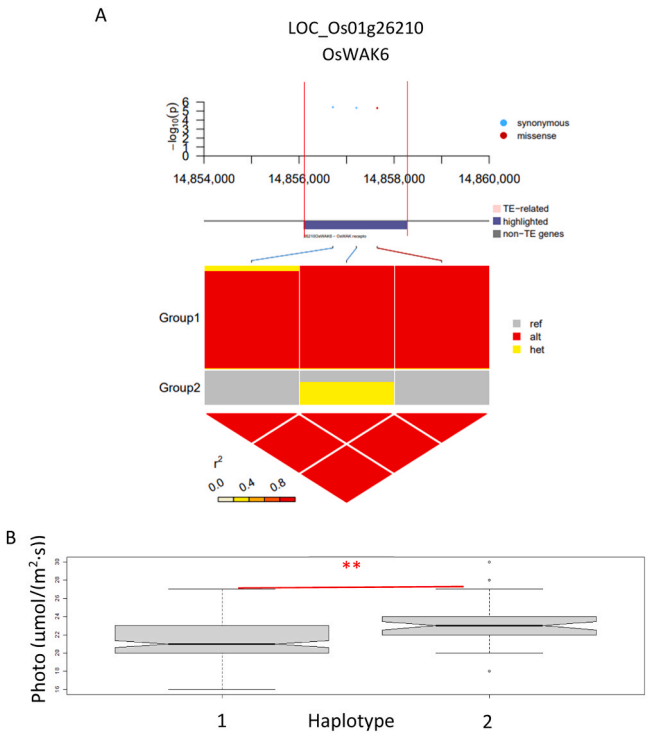

Fig. 8. Haplotype analyses of the LOC_Os01g26210 candidate gene at qPHOTO-1–2. (A) Linkage disequilibrium (LD) block surrounding the region of LOC_Os01g26210 gene at qPHOTO-1–2. (B) Boxplots for photosynthetic rate (Photo) 2016 based on haplotypes for LOC_Os01g26210. ** indicates the level of significant different (T-test, $P < 0.001$) between the groups. (C) The SNP positions and alleles, the number of accessions and mean value of photosynthetic rate (Photo) for each haplotype.

qPHOTO-4–1 and qPHOTO-4–2 overlapped with chlorophyll content QTLs qCCFJ-4 and QTAROqtl-1002, respectively [61]. Two chloroplast precursors, CRS2-associated factor 2 (LOC_Os01g21990) and CRS2-associated factor 1 (LOC_Os01g31110) are in the region of qPHOTO-1–1. Stress response genes are also found in qPHOTO loci, such as the ENHANCED DOWNY MILDEW 2 (EDM2) gene (LOC_Os01g32710) at qPHOTO-1–4 and a universal stress protein domain containing protein (LOC_Os01g32780) at qPHOTO-1–5. The region of qPHOTO-1–1 contains a cell death related gene, respiratory burst oxidase (LOC_Os01g25820), and a stress response gene,

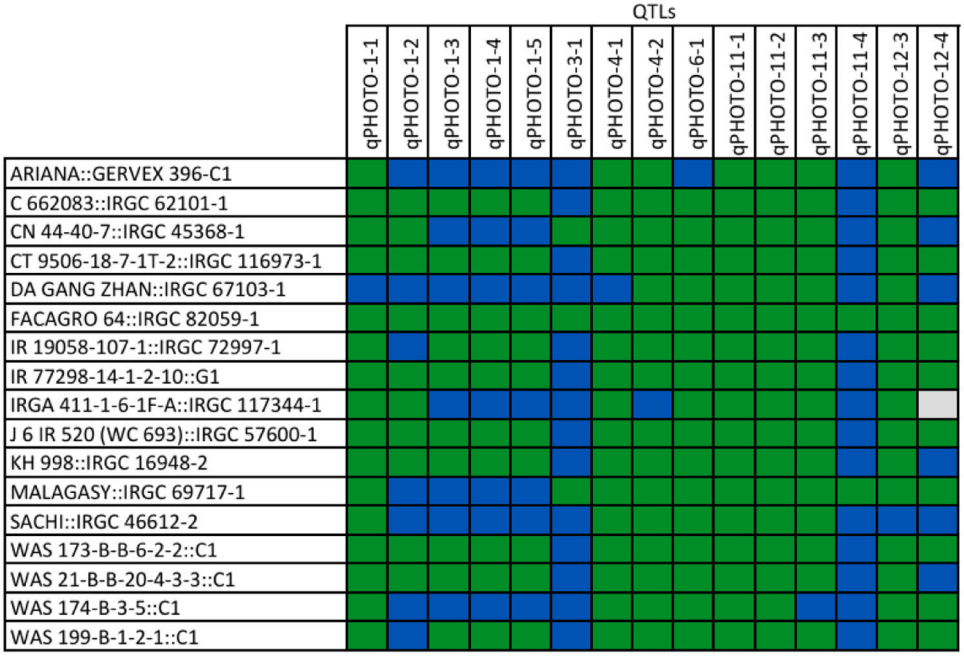

Fig. 9. Haplotype analysis of qPHOTO-associated QTLs. Green cells indicate the 17 high-photosynthesis accessions belonging to a haplotype group exhibiting a significantly ($p < 0.05$) higher average photosynthetic rate compared with the alternative haplotype group (blue). Gray cells indicate accessions belonging to haplotype groups that are not significantly different from either the high- or low-photosynthetic haplotype groups.

cytochrome P450 72A1 (LOC_Os01g29150). The observation of overlapping QTLs among different photosynthetic traits, such as qWUE-2–1/qTRMMOL-2–2, qCOND-3–1/qTRMMOL-3–1, and qPHOTO-4–1/qCOND-4–2/qTRMMOL-4–1, suggests that certain photosynthetic traits may be regulated by shared or common QTLs. This corresponds with the high correlations observed between these traits (Figure S1). Our results indicate that there are individual genes associated with variation in multiple traits from different trait groups, suggesting a degree of conservation in terms of the genes that regulate photosynthesis. The analysis has also led to the identification of several genes with a putative or unknown function, reflecting that GWAS may be used to help characterize unknown genes. Although the precise mechanism of action through which these genes regulate photosynthetic traits has yet to be established, these results are an encouraging validation of the method. It also demonstrates the potential to understand the level of genetic variation within known photosynthetic genes.

High-throughput phenotyping using drone imaging systems is well-suited to characterizing diversity panels and conducting time-course measurements that would be prohibitive using manual and destructive approaches. A previous study demonstrated that the high-throughput measurement NDVI correlated with key phenotypic traits such as yield, biomass, days to heading (DTH), and plant growth [20]. Prior research has primarily focused on utilizing drone imaging systems to detect or predict rice yield and assess plant health in relation to biotic and abiotic stresses [62–64]. In our study, we extended the application of drone imaging systems by exploring the correlation between UAV-derived data and rice physiological characteristics, such as photosynthetic capacity, stomatal density, and morphological traits. In all three years of experiments, we observed that photosynthetic rate (PHOTO) and stomatal conductance (COND) were negatively correlated with NDVI during the early tillering stage (before 55 days after transplanting). This negative correlation indicates that NDVI can serve as a reliable indicator of photosynthetic activity in paddy fields during this critical growth phase. Our data also revealed that NDVI values were positively correlated with plant height, leaf length, and DTH, but negatively correlated with canopy temperature (Fig. 3; Figure S2). The increase and decrease in NDVI can serve as indicators of an accession's growth or senescence stages. The relative growth rates (RGR) and senescence rates (SR) based on the changes of NDVI correlated with various agronomic traits, such as leaf length (LLT), canopy number (CUNO), days to heading (DTH), grain yield, stomatal density (SD), and plant height (HT), demonstrating another application of NDVI. A cooler canopy temperature , reflecting enhanced transpirational cooling via stomatal conductance, is associated with higher photosynthetic rates and yield [13,65]. Consistently, canopy temperature in rice was negatively correlated with stomatal conductance, plant height, biomass, and yield. In addition to correlation analysis, we assessed the predictive ability of HTP derived indices on photosynthetic traits via penalized regression models. We observed strong variation in R^2 across years for SD, WUE, and Photo, with the highest R^2 values exhibited in 2016 across all traits except WUE. Together, these results suggest that UAV-derived traits such as early-season NDVI trajectories and canopy temperature can be used as first-pass screening tools to identify genotypes with favorable photosynthetic and stomatal characteristics, which can then be prioritized for targeted physiological measurements and marker-assisted selection. However, while higher R^2 values could be considered suitable for ranking, the range of out-of-fold predicted values for SD was consistently narrower than that of observed values (Fig. S26), indicating limitations of this approach for predicting absolute values for individual genotypes.

Additionally, canopy temperature was significantly correlated with stomatal density (SD) (Fig. 3), supporting its use as a proxy for stomatal traits. The QTL regions for canopy temperature contain several genes involved in cell development, hormone synthesis and stress response. For example, qCT-1–3 contains a cytokinin dehydrogenase precursor gene (LOC_Os01g56810) that is involved in plant growth and developmental processes [66], as well as several stress response genes (LOC_Os01g57270, LOC_Os01g57280, LOC_Os01g57310, LOC_Os01g57340, LOC_Os01g57450, LOC_Os01g57460, LOC_Os01g57730, LOC_Os01g57770, LOC_Os01g58420, LOC_Os01g58550, LOC_Os01g58610, LOC_Os01g58730, LOC_Os01g58740). The region of qCT-1–6 contains a cytokinin glycosyltransferase, cytokinin-N-glucosyltransferase 1 (LOC_Os01g59100), which is involved in cytokinin synthesis and accumulation in rice [67]. The overlapping regions of qCT-1–1 and qPHOTO-1–4 contain a mitogen-activated protein kinase kinase gene OsMKK6 (LOC_Os01g32660) involved in cold tolerance [68]. The regions of aCT-1–4 and qHT1–1–1 overlap and contain an indole-3-acetic acid-amido synthetase, OsGH3.1 (LOC_Os01g57610), which is related to cell growth and seed germination, and a transcription factor, OsEDL3 (LOC_Os01g58850), which was upregulated during drought stress [69]. With further testing and validation, the QTLs identified in our study could serve as markers in breeding programs to select rice plants with higher yield and adaptability to future climate conditions.

Among the identified QTLs associated with photosynthetic traits, qPHOTO-1–2 was particularly notable for harboring haplotypes within the gene region of LOC_Os01g26210, which encodes OsWAK6, a wall-associated receptor-like kinase. Haplotype analysis revealed that Haplotype 2, which carries a missense SNP, was significantly associated with a higher photosynthetic rate compared to Haplotype 1, suggesting a potential functional impact of OsWAK6 on photosynthetic performance (Fig. 8). OsWAK6 belongs to the OsWAK gene family, members of which are known to mediate responses to biotic and abiotic stresses, as well as contribute to plant development and reproduction [70,71]. While most studies have emphasized their roles in disease resistance and stress signaling, our results suggest that OsWAK6 may also influence photosynthetic efficiency, representing a previously underexplored function. One of the candidate genes at qTRMMOL-4–1, identified through haplotype variation analysis, LOC_Os04g32920 (OsHAK1), encodes a high-affinity potassium (K^+) transporter essential for maintaining potassium uptake and homeostasis in rice [72]. OsHAK1 plays a crucial role in plant growth, root development, pollen viability, and fertility, as knockout of OsHAK1 leads to reduced root growth and impaired sugar metabolism [73]. In our haplotype variation analysis, Haplotype 1, which carries a missense mutation in OsHAK1, exhibited a lower transpiration rate (Fig. 7). Furthermore, QTL co-location analysis revealed that qTRMMOL-4–1 overlaps with qCOND-4–2, qGRAIN_YIELD-4–1, and qHI-4–4, suggesting a broader role in plant performance. Together, these findings support OsHAK1 as a candidate gene involved in regulating rice transpiration rate, with potential implications for water-use efficiency and stress response. Future studies should aim to functionally characterize OsHAK1 in the context of transpiration and water-use efficiency by analyzing both mutant and overexpression lines under different environmental conditions. These approaches will help clarify its role and potential utility in improving drought tolerance and yield stability in rice.

5. Conclusions

By integrating manual physiological measurements with UAV-based high-throughput phenotyping (HTP), this study revealed robust relationships among photosynthetic traits, NDVI, and canopy temperature in rice under field conditions. This integrated framework enabled the identification of accessions with superior photosynthetic performance and associated genomic loci with clear relevance for crop improvement. Where such loci are absent from current elite breeding pools, they represent valuable targets for introgression into high-yielding cultivars. Notably, two candidate genes, OsWAK6 and OsHAK1, implicated in the regulation of photosynthesis and transpiration, emerged as promising targets for future functional validation. We view this work as establishing a baseline resource for dissecting the genetic and physiological architecture of photosynthetic performance in rice. While the present dataset provides biologically meaningful insights, the application of

more advanced machine-learning–based predictive approaches will likely require larger and more diverse populations. Together, our results provide a foundation for developing high-productivity, climate-resilient rice varieties and contribute to the advancement of sustainable agricultural systems.

Authors' contribution

KLM designed the field study. HL, WPQ, and KLM designed the analyses. HL, MJD, and MRL analyzed the phenotypic data. MMEBN and PAM conducted the field experiments. SK collected and processed the drone data. HL conducted the AMMI. DC conducted penalized regression models tests. HL and DC conducted the GWAS. DC and KLM performed the RicePilaf analysis. HL, DC, SK, AH, WPQ, and KLM interpreted the data and developed the manuscript.

Funding

This research was partially supported by CGIAR Research Program to Global Rice Science Partnership (GRiSP) and the Ministry of Agriculture (MOA), grant no. 115AS-1.2.3-AS-04.

Declaration of Competing Interest

The authors have no conflicts of interest to declare.

Acknowledgements

We acknowledge the molecular genetics team of the T.T. Chang Genetic Resources Center for their support in field management and the collection of agro-morphological traits. We thank the field and laboratory technicians of the IRRI C4 Rice team for their assistance with data collections. We thank Irma Canicosa for her help with photosynthesis measurements.

Appendix A. Supporting information

Supplementary data associated with this article can be found in the online version at doi:10.1016/j.cpb.2026.100613.

Data availability

Data will be made available on request.

References

[1] FAO, The future of food and agriculture – Alternative pathways to 2050, Rome (2018).
[2] F. Seck, G. Covarrubias-Pazaran, T. Gueye, J. Bartholome, Realized genetic gain in rice: achievements from breeding programs, Rice (N. Y) 16 (2023) 61, https://doi.org/10.1186/s12284-023-00677-6.
[3] J. Gu, X. Yin, T.J. Stomph, P.C. Struik, Can exploiting natural genetic variation in leaf photosynthesis contribute to increasing rice productivity? A simulation analysis, Plant Cell Environ. 37 (2014) 22–34, https://doi.org/10.1111/pce.12173.
[4] S. Covshoff, J.M. Hibberd, Integrating C4 photosynthesis into C3 crops to increase yield potential, Curr. Opin. Biotechnol. 23 (2012) 209–214, https://doi.org/10.1016/j.copbio.2011.12.011.
[5] S.P. Long, A. Marshall-Colon, X.G. Zhu, Meeting the global food demand of the future by engineering crop photosynthesis and yield potential, Cell 161 (2015) 56–66, https://doi.org/10.1016/j.cell.2015.03.019.
[6] J. Kromdijk, K. Głowacka, L. Leonelli, S.T. Gabilly, M. Iwai, K.K. Niyogi, S.P. Long, Improving photosynthesis and crop productivity by accelerating recovery from photoprotection, Science 354 (2016) 857–861, https://doi.org/10.1126/science.aai8878.
[7] K. Sakoda, S. Adachi, W. Yamori, Y. Tanaka, Towards improved dynamic photosynthesis in C3 crops by utilizing natural genetic variation, J. Exp. Bot. 73 (2022) 3109–3121, https://doi.org/10.1093/jxb/erac100.
[8] S.M. Whitney, R.L. Houtz, H. Alonso, Advancing our understanding and capacity to engineer nature's CO2-sequestering enzyme, Rubisco, Plant Physiol. 155 (2011) 27–35, https://doi.org/10.1104/pp.110.164814.
[9] A. Makino, T. Mae, Photosynthesis and Plant Growth at Elevated Levels of CO2, Plant Cell Physiol. 40 (1999) 999–1006, https://doi.org/10.1093/oxfordjournals.pcp.a029493.
[10] M.U.F. Kirschbaum, Does Enhanced Photosynthesis Enhance Growth? Lessons Learned from CO2 Enrichment Studies, Plant Physiol. 155 (2010) 117–124, https://doi.org/10.1104/pp.110.166819.
[11] E.A. Ainsworth, S.P. Long, What have we learned from 15 years of free-air CO2 enrichment (FACE)? A meta-analytic review of the responses of photosynthesis, canopy properties and plant production to rising CO2, N. Phytol. 165 (2005) 351–371, https://doi.org/10.1111/j.1469-8137.2004.01224.x.
[12] V.O. Sadras, C. Lawson, A. Montoro, Photosynthetic traits in Australian wheat varieties released between 1958 and 2007, Field Crops Res. 134 (2012) 19–29, https://doi.org/10.1016/j.fcr.2012.04.012.
[13] R.A. Fischer, D. Rees, K.D. Sayre, Z.M. Lu, A.G. Condon, A.L. Saavedra, Wheat yield progress associated with higher stomatal conductance and photosynthetic rate, and cooler canopies, Crop Sci. 38 (1998) 1467–1475, https://doi.org/10.2135/cropsci1998.0011183X003800060011x.
[14] L.G. Acevedo-Siaca, R. Coe, Y. Wang, J. Kromdijk, W.P. Quick, S.P. Long, Variation in photosynthetic induction between rice accessions and its potential for improving productivity, N. Phytol. 227 (2020) 1097–1108, https://doi.org/10.1111/nph.16454.
[15] R. Giuliani, N. Koteyeva, E. Voznesenskaya, M.A. Evans, A.B. Cousins, G. E. Edwards, Coordination of leaf photosynthesis, transpiration, and structural traits in rice and wild relatives (Genus Oryza), Plant Physiol. 162 (2013) 1632–1651, https://doi.org/10.1104/pp.113.217497.
[16] S.B. Cowling, P. Treeintong, J. Ferguson, H. Soltani, R. Swarup, S. Mayes, E. H. Murchie, Out of Africa: characterizing the natural variation in dynamic photosynthetic traits in a diverse population of African rice (Oryza glaberrima), J. Exp. Bot. 73 (2022) 3283–3298, https://doi.org/10.1093/jxb/erab459.
[17] The rice genomes project, The 3,000 rice genomes project 3 Gigascience2014, 710.1186/2047-217X-3-7.
[18] R.T. Furbank, M. Tester, Phenomics–technologies to relieve the phenotyping bottleneck, Trends Plant Sci. 16 (2011) 635–644, https://doi.org/10.1016/j.tplants.2011.09.005.
[19] D. Deery, J. Jimenez-Berni, H. Jones, X. Sirault, R. Furbank, Proximal remote sensing buggies and potential applications for field-based phenotyping, Agronomy 4 (2014) 349–379, https://doi.org/10.3390/agronomy4030349.
[20] P. Tanger, S. Klassen, J.P. Mojica, J.T. Lovell, B.T. Moyers, M. Baraoidan, M. E. Naredo, K.L. McNally, J. Poland, D.R. Bush, H. Leung, J.E. Leach, J.K. McKay, Field-based high throughput phenotyping rapidly identifies genomic regions controlling yield components in rice, Sci. Rep. 7 (2017) 42839, https://doi.org/10.1038/srep42839.
[21] J.K. Robson, J.N. Ferguson, L. McAusland, J.A. Atkinson, C. Tranchant-Dubreuil, P. Cubry, F. Sabot, D.M. Wells, A.H. Price, Z.A. Wilson, E.H. Murchie, Chlorophyll fluorescence-based high-throughput phenotyping facilitates the genetic dissection of photosynthetic heat tolerance in African (Oryza glaberrima) and Asian (Oryza sativa) rice, J. Exp. Bot. 74 (2023) 5181–5197, https://doi.org/10.1093/jxb/erad239.
[22] R.R. Mir, M. Reynolds, F. Pinto, M.A. Khan, M.A. Bhat, High-throughput phenotyping for crop improvement in the genomics era, Plant Sci. 282 (2019) 60–72, https://doi.org/10.1016/j.plantsci.2019.01.007.
[23] A. Ac, Z. Malenovsky, J. Hanus, I. Tomaskova, O. Urban, M.V. Marek, Near-distance imaging spectroscopy investigating chlorophyll fluorescence and photosynthetic activity of grassland in the daily course, Funct. Plant Biol. 36 (2009) 1006–1015, https://doi.org/10.1071/FP09154.
[24] X. Huang, Y. Zhao, X. Wei, C. Li, A. Wang, Q. Zhao, W. Li, Y. Guo, L. Deng, C. Zhu, D. Fan, Y. Lu, Q. Weng, K. Liu, T. Zhou, Y. Jing, L. Si, G. Dong, T. Huang, T. Lu, Q. Feng, Q. Qian, J. Li, B. Han, Genome-wide association study of flowering time and grain yield traits in a worldwide collection of rice germplasm, Nat. Genet 44 (2011) 32–39, https://doi.org/10.1038/ng.1018.
[25] W. Chen, Y. Gao, W. Xie, L. Gong, K. Lu, W. Wang, Y. Li, X. Liu, H. Zhang, H. Dong, W. Zhang, L. Zhang, S. Yu, G. Wang, X. Lian, J. Luo, Genome-wide association analyses provide genetic and biochemical insights into natural variation in rice metabolism, Nat. Genet 46 (2014) 714–721, https://doi.org/10.1038/ng.3007.
[26] K. Chigira, N. Kojima, M. Yamasaki, K. Yano, S. Adachi, T. Nomura, M. Jiang, K. Katsura, T. Ookawa, Landraces of temperate japonica rice have superior alleles for improving culm strength associated with lodging resistance, Sci. Rep. 10 (2020) 19855, https://doi.org/10.1038/s41598-020-76949-8.
[27] S.T. Cu, N.I. Warnock, J. Pasuquin, M. Dingkuhn, J. Stangoulis, A high-resolution genome-wide association study of the grain ionome and agronomic traits in rice Oryza sativa subsp. indica, Sci. Rep. 11 (2021) 19230, https://doi.org/10.1038/s41598-021-98573-w.
[28] S. Honda, A. Imamura, Y. Seki, K. Chigira, M. Iwasa, K. Hayami, T. Nomura, S. Ohkubo, T. Ookawa, A.J. Nagano, M. Matsuoka, Y. Tanaka, S. Adachi, Genome-wide association study of leaf photosynthesis using a high-throughput gas exchange system in rice, Photosynth. Res. 159 (2024) 17–28, https://doi.org/10.1007/s11120-023-01065-3.
[29] Bioversity International, International Rice Research Institute (IRRI), The Africa Rice Center (WARDA), Descriptors for wild and cultivated rice (Oryza spp.), Bioversity Int. 63 (2007).
[30] J. Chatterjee, V. Thakur, R. Nepomuceno, R.A. Coe, J. Dionora, A. Elmido-Mabilangan, A.D. Llave, A.M.D. Reyes, A.N. Monroy, I. Canicosa, A. Bandyopadhyay, K.K. Jena, D.S. Brar, W.P. Quick, Natural Diversity in Stomatal Features of Cultivated and Wild Oryza Species, Rice (N. Y) 13 (2020) 58, https://doi.org/10.1186/s12284-020-00417-0.

[31] R Core Team. R: A language and environment for statistical computing, R Foundation for Statistical Computing, Vienna, Austria, 2015. https://www.R-project.org/.
[32] X. Zhou, M. Stephens, Genome-wide efficient mixed-model analysis for association studies, Nat. Genet 44 (2012) 821–824, https://doi.org/10.1038/ng.2310.
[33] ⟨https://snp-seek.irri.org⟩ Edited by: Rice SNP-Seek Database; accessed on 3 May 2021.
[34] L. Mansueto, R.R. Fuentes, F.N. Borja, J. Detras, J.M. Abriol-Santos, D. Chebotarov, M. Sanciangco, K. Palis, D. Copetti, A. Poliakov, I. Dubchak, V. Solovyev, R. A. Wing, R.S. Hamilton, R. Mauleon, K.L. McNally, N. Alexandrov, Rice SNP-seek database update: new SNPs, indels, and queries, Nucleic Acids Res 45 (2017) D1075–d1081, https://doi.org/10.1093/nar/gkw1135.
[35] D.R. Wang, F.J. Agosto-Pérez, D. Chebotarov, Y. Shi, J. Marchini, M. Fitzgerald, K. L. McNally, N. Alexandrov, S.R. McCouch, An imputation platform to enhance integration of rice genetic resources, Nat. Commun. 9 (2018) 3519, https://doi.org/10.1038/s41467-018-05538-1.
[36] S. Purcell, B. Neale, K. Todd-Brown, L. Thomas, M.A. Ferreira, D. Bender, J. Maller, P. Sklar, P.I. de Bakker, M.J. Daly, P.C. Sham, PLINK: a tool set for whole-genome association and population-based linkage analyses, Am. J. Hum. Genet 81 (2007) 559–575, https://doi.org/10.1086/519795.
[37] C.C. Chang, C.C. Chow, L.C. Tellier, S. Vattikuti, S.M. Purcell, J.J. Lee, Second-generation PLINK: rising to the challenge of larger and richer datasets, GigaScience 4 (2015), https://doi.org/10.1186/s13742-015-0047-8.
[38] J. Li, L. Ji, Adjusting multiple testing in multilocus analyses using the eigenvalues of a correlation matrix, Heredity 95 (2005) 221–227, https://doi.org/10.1038/sj.hdy.6800717.
[39] X. Gao, J. Starmer, E.R. Martin, A multiple testing correction method for genetic association studies using correlated single nucleotide polymorphisms, Genet Epidemiol. 32 (2008) 361–369, https://doi.org/10.1002/gepi.20310.
[40] T. Lee, T. Oh, S. Yang, J. Shin, S. Hwang, C.Y. Kim, H. Kim, H. Shim, J.E. Shim, P. C. Ronald, I. Lee, RiceNet v2: an improved network prioritization server for rice genes, Nucleic Acids Res. 43 (2015) W122–W127, https://doi.org/10.1093/nar/gkv253.
[41] A.M.S. Shrestha, M.E.M. Gonzales, P.C.L. Ong, P. Larmande, H.-S. Lee, J.-U. Jeung, A. Kohli, D. Chebotarov, R.P. Mauleon, J.-S. Lee, K.L. McNally, RicePilaf: a post-GWAS/QTL dashboard to integrate pangenomic, coexpression, regulatory, epigenomic, ontology, pathway, and text-mining information to provide functional insights into rice QTLs and GWAS loci, GigaScience 13 (2024), https://doi.org/10.1093/gigascience/giae013.
[42] T. Nepusz, H. Yu, A. Paccanaro, Detecting overlapping protein complexes in protein-protein interaction networks, Nat. Methods 9 (2012) 471–472, https://doi.org/10.1038/nmeth.1938.
[43] R Core Team. R: A Language and Environment for Statistical Computing, R Foundation for Statistical Computing, Vienna, Austria, 2024. https://www.R-project.org/.
[44] T. Wei, V. Simko, M. Levy, Y. Xie, Y. Jin, J. Zemla, M. Freidank, J. Cai and T. Protivinsky: Visualization of a Correlation Matrix. Edited by; 2024.
[45] Q. Liao, D. Chebotarov, M.S. Islam, M.R. Quintana, M.A. Natividad, M. De Ocampo, J.C. Beredo, R.O. Torres, Z. Zhang, H. Song, A.H. Price, K.L. McNally, A. Henry, Aus rice root architecture variation contributing to grain yield under drought suggests a key role of nodal root diameter class, Plant Cell Environ. 45 (2022) 854–870, https://doi.org/10.1111/pce.14272.
[46] F. De Mendiburu Delgado: Una herramienta de analisis estadistico para la investigacion agricola. Edited by: Universidad Nacional de Ingenieria (UNI-PERU); 2009.
[47] J.H. Friedman, T. Hastie, R. Tibshirani, Regularization Paths for Generalized Linear Models via Coordinate Descent, J. Stat. Softw. 33 (2010) 1–22, https://doi.org/10.18637/jss.v033.i01.
[48] M.W. Kuhn, Hadley: Tidymodels: a collection of packages for modeling and machine learning using tidyverse principles. Edited by; 2020.
[49] M. Kuhn: tune: Tidy Tuning Tools., edn R package version 2.0.1. Edited by; 2025.
[50] H. Chen, X Zhao, L. Zhai, K. Shao, K. Jiang, C. Shen, K. Chen, S. Wang, Y. Wang, J. Xu, Genetic bases of the stomata-related traits revealed by a genome-wide association analysis in rice (Oryza sativa L.), Front. Genet. 11 (2020) 611, https://doi.org/10.3389/fgene.2020.00611.
[51] P. Li, J. Jiang, G. Zhang, S. Miao, J. Lu, Y. Qian, X. Zhao, W. Wang, X. Qiu, F. Zhang, J. Xu, Integrating GWAS and transcriptomics to identify candidate genes conferring heat tolerance in rice, Front. Plant Sci. 13 (2023) 2022, https://doi.org/10.3389/fpls.2022.1102938.
[52] M. Faralli, T. Lawson, Natural genetic variation in photosynthesis: an untapped resource to increase crop yield potential? Plant J. 101 (2020) 518–528, https://doi.org/10.1111/tpj.14568.
[53] J. Gu, X. Yin, P.C. Struik, T.J. Stomph, H. Wang, Using chromosome introgression lines to map quantitative trait loci for photosynthesis parameters in rice (Oryza sativa L.) leaves under drought and well-watered field conditions, J. Exp. Bot. 63 (2012) 455–469, https://doi.org/10.1093/jxb/err292.
[54] J. Gu, X. Yin, T.J. Stomph, H. Wang, P.C. Struik, Physiological basis of genetic variation in leaf photosynthesis among rice (Oryza sativa L.) introgression lines under drought and well-watered conditions, J. Exp. Bot. 63 (2012) 5137–5153, https://doi.org/10.1093/jxb/ers170.
[55] S. Adachi, T. Yamamoto, T. Nakae, M. Yamashita, M. Uchida, R. Karimata, N. Ichihara, K. Soda, T. Ochiai, R. Ao, C. Otsuka, R. Nakano, T. Takai, T. Ikka, K. Kondo, T. Ueda, T. Ookawa, T. Hirasawa, Genetic architecture of leaf photosynthesis in rice revealed by different types of reciprocal mapping populations, J. Exp. Bot. 70 (2019) 5131–5144, https://doi.org/10.1093/jxb/erz303.
[56] L. Wu, H.J. de Boer, Z. Zixiao, X. Chen, Y. Shi, S. Peng, F. Wang, The coordinated increase in stomatal density and vein dimensions during genetic improvement in rice, Agron. J. 112 (2020) 2791–2804, https://doi.org/10.1002/agj2.20180.
[57] D. Roche, Stomatal Conductance Is Essential for Higher Yield Potential of C3 Crops, Crit. Rev. Plant Sci. 34 (2015) 429–453, https://doi.org/10.1080/07352689.2015.1023677.
[58] X. Yin, A.K. Biswal, J. Dionora, K.M. Perdigon, C.P. Balahadia, S. Mazumdar, C. Chater, H.C. Lin, R.A. Coe, T. Kretzschmar, J.E. Gray, P.W. Quick, A. Bandyopadhyay, CRISPR-Cas9 and CRISPR-Cpf1 mediated targeting of a stomatal developmental gene EPFL9 in rice, Plant Cell Rep. 36 (2017) 745–757, https://doi.org/10.1007/s00299-017-2118-z.
[59] R.S. Caine, X. Yin, J. Sloan, E.L. Harrison, U. Mohammed, T. Fulton, A.K. Biswal, J. Dionora, C.C. Chater, R.A. Coe, A. Bandyopadhyay, E.H. Murchie, R. Swarup, W. P. Quick, J.E. Gray, Rice with reduced stomatal density conserves water and has improved drought tolerance under future climate conditions, N. Phytol. 221 (2019) 371–384, https://doi.org/10.1111/nph.15344.
[60] Y. Gao, X. Xiang, Y. Zhang, Y. Cao, B. Wang, Y. Zhang, C. Wang, M. Jiang, W. Duan, D. Chen, X. Zhan, S. Cheng, Q. Liu, L. Cao, Disruption of OsPHD1, Encoding a UDP-Glucose Epimerase, Causes JA Accumulation and Enhanced Bacterial Blight Resistance in Rice, Int. J. Mol. Sci. 23 (2022) 751.
[61] J.-i Yonemaru, T. Yamamoto, S. Fukuoka, Y. Uga, K. Hori, M. Yano, Q-TARO: QTL Annotation Rice Online Database, Rice 3 (2010) 194–203, https://doi.org/10.1007/s12284-010-9041-z.
[62] B. Duan, S. Fang, R. Zhu, X. Wu, S. Wang, Y. Gong, Y. Peng, Remote Estimation of Rice Yield With Unmanned Aerial Vehicle (UAV) Data and Spectral Mixture Analysis, Front Plant Sci. 10 (2019) 204, https://doi.org/10.3389/fpls.2019.00204.
[63] G. Carracelas, C. Ballester, C. Marchesi, A. Roel, J. Hornbuckle, Assessing Drone-Based Remote Sensing Indices for Monitoring Rice Nitrogen Plant Status Under Different Irrigation Techniques, Agronomy 14 (2024) 2976.
[64] T. Gill, S.K. Gill, D.K. Saini, Y. Chopra, J.P. de Koff, K.S. Sandhu, A comprehensive review of high throughput phenotyping and machine learning for plant stress phenotyping, Phenomics 2 (2022) 156–183, https://doi.org/10.1007/s43657-022-00048-z.
[65] R.E. Sharwood, W.P. Quick, D. Sargent, G.M. Estavillo, V. Silva-Perez, R. T. Furbank, Mining for allelic gold: finding genetic variation in photosynthetic traits in crops and wild relatives, J. Exp. Bot. 73 (2022) 3085–3108, https://doi.org/10.1093/jxb/erac081.
[66] C. Rong, Y. Liu, Z. Chang, Z. Liu, Y. Ding, C. Ding, Cytokinin oxidase/dehydrogenase family genes exhibit functional divergence and overlap in rice growth and development, especially in control of tillering, J. Exp. Bot. 73 (2022) 3552–3568, https://doi.org/10.1093/jxb/erac088.
[67] P. Li, K. Lei, Y. Li, X. He, S. Wang, R. Liu, L. Ji, B. Hou, Identification and characterization of the first cytokinin glycosyltransferase from rice, Rice (N. Y) 12 (2019) 19, https://doi.org/10.1186/s12284-019-0279-9.
[68] J. Chen, L. Wang, M. Yuan, Update on the Roles of Rice MAPK Cascades, Int J. Mol. Sci. 22 (2021), https://doi.org/10.3390/ijms22041679.
[69] E.L. Baggs, J.G. Monroe, A.S. Thanki, R. O'Grady, C. Schudoma, W. Haerty, K. V. Krasileva, Convergent Loss of an EDS1/PAD4 Signaling Pathway in Several Plant Lineages Reveals Coevolved Components of Plant Immunity and Drought Response, Plant Cell 32 (2020) 2158–2177, https://doi.org/10.1105/tpc.19.00903.
[70] S. Zhang, C. Chen, L. Li, L. Meng, J. Singh, N. Jiang, X.W. Deng, Z.H. He, P. G. Lemaux, Evolutionary expansion, gene structure, and expression of the rice wall-associated kinase gene family, Plant Physiol. 139 (2005) 1107–1124, https://doi.org/10.1104/pp.105.069005.
[71] W. Huluka, L. Kumsa, Analysis of rice (Oryza sativa L. ssp. Japonica) wall associated receptor-like protein kinase gene's promoter region and regulatory elements, Curr. Plant Biol. 31 (2022) 100254, https://doi.org/10.1016/j.cpb.2022.100254.
[72] G. Chen, Q. Hu, L. Luo, T. Yang, S. Zhang, Y. Hu, L. Yu, G. Xu, Rice potassium transporter OsHAK1 is essential for maintaining potassium-mediated growth and functions in salt tolerance over low and high potassium concentration ranges, Plant Cell Environ. 38 (2015) 2747–2765, https://doi.org/10.1111/pce.12585.
[73] G. Chen, Y. Zhang, B. Ruan, L. Guo, D. Zeng, Z. Gao, L. Zhu, J. Hu, D. Ren, L. Yu, G. Xu, Q. Qian, OsHAK1 controls the vegetative growth and panicle fertility of rice by its effect on potassium-mediated sugar metabolism, Plant Sci. 274 (2018) 261–270, https://doi.org/10.1016/j.plantsci.2018.05.034.